

PanAfGeo

Pan-African Support
to Geological Sciences and
Technology Africa-EU Partnership

Appui panafricain aux géosciences
du partenariat Afrique-UE

Apoio pan-africano às geociências
da parceria África-UE

PanAfGeo2 training WPA-U5 in Uganda, 2024

“Field Geoscientific Mapping”



Excursion Guide to the Entebbe and Kabale area, SW Uganda

From 27 February to 26 March 2024



Text written and compiled by

Veronika Štědrá (ed.), Vladimír Žáček, Nelson Birungi, Pavel Pitra, Joseph Aiykobua, Zuzana Tasáryová, Deus K. Muhwezi, Sudan U. Birungi, Joseph Nyago, and Jan Jelének.



Entebbe, Uganda, 2024



PanAfGeo

Pan-African Support
to Geological Sciences and
Technology Africa-EU Partnership

Appui panafricain aux géosciences
du partenariat Afrique-UE

Apoio pan-africano às geociências
da parceria África-UE

TABLE OF CONTENTS

Foreword	3
1. INTRODUCTION TO THE REGIONAL GEOLOGY OF UGANDA	4
1.1. Geological framework of Uganda (GSD)	4
1.2. Regional tectono-metamorphic framework of the SW part of Uganda	5
1.3. Summary of geological setting of the Kabale region.....	6
1.4. Road geology between Entebbe and Kabale – Monday March 4, 2024	8
2. METHODOICAL EXCURSION	9
2.1 Outline.....	9
2.2 Methodical excursion No. 1 – Geology and lithology	9
2.3 Methodical Excursion No. 2 – Structural Geology	13
2.4 Geophysical survey methods practice	17
2.4.1. Aim of the survey	17
2.4.2. Survey area.....	17
2.4.3. Methodology.....	18
2.4.4. Survey design.....	18
2.4.5. Field	19
2.4.6. Geophysical data processing.....	22
2.4.7. Results of the geophysical survey.....	28
2.5. Geochemical sampling practice.....	29
2.5.1. Stream sediment sampling.....	29
2.5.2. Soil sampling.....	29
2.5.3. Biogeochemical sampling	30
2.5.4. Heavy mineral sampling (HM)	30
3. MINE EXCURSIONS	31
3.1. Iron mine Karukura	31
3.2. The tin mine of Mwerasandu, SE of Ntungamo.....	31
3.3. Tungsten-bearing pegmatite near Kacherere.....	32
4. MAPPING AREAS/POLYGONS	34

5. REMOTE SENSING AND MOBILE METHODS.....	35
5.1 Field data collection using mobile app.....	35
5.2 Introduction to remote sensing methods.....	35
6. PLATES 1–7: LITHOLOGY OF THE TRAINING AREA.....	37
Plate 1 – Mesoproterozoic sediments of the Kabale area	37
Plate 2 – Neoproterozoic rocks of the Kabale area	38
Plate 3 – Granitoids of the Neoproterozoic age	39
Plate 4 – Dyke rocks	40
Plate 5 – EARS volcanic rocks of Neogene to Quaternary age	41
Plate 6 – Quaternary sedimentary cover	42
Plate 7 – Thin sections from Kabale area rocks	43
7. SELECTED BIBLIOGRAPHY.....	44
8. WPA-U5 PARTICIPANTS	46

Foreword

The second phase of the international programme PanAfGeo2 (2021–2024) funded by EU and twelve European geological surveys is targeted at the practical improvement and capacity building for the staff of geological surveys of African states. Its “Work Package A” is focused on practical skills in field geoscientific mapping and represents the most variegated work package of seven other work packages included in the programme. Similar trainings were held in Ethiopia, Namibia, Morocco, Cameroon, Malawi and Senegal during the previous stages of the programme, under the leadership by the Czech Geological Survey, Prague.

The training of the “Field Geoscientific Mapping” in Uganda (WPAU5) closed the PanAfGeo2 programme; it was focused on the person-to-person intense teaching of the logistic, geoscientific, remote sensing, GIS, and interpretation methods leading to the construction of geological maps at different scales, of which the 1: 25 000 was applied to the training. An important role in the mapping process was played by instrumental methods, remote sensing and GIS including mobile applications that formed an essential part of the training.

The mapping training was prepared and launched in this country for the first time, taking an advantage of status of the Geological Survey Department of Uganda as the coordinating local partner of the Work Package A.

The outskirts of Kabale town in the SW part of the country, where the local branch of the GSD resides, hosted the practical field methodical and mapping parts. The introductory and interpretation parts of the training were held in Entebbe, with the support of the GSD staff experts.

This Field Guide documents the activities of this specific mapping training held in 2024. It should provide a record on the field part of the training for all the participants from 14 countries and for the lecturers. It may also provide a useful practical information on geology of the Kabale District of Uganda for future students, teachers of Earth sciences or even visitors focused on geotourism.

Veronika Štědrá, CGS Prague

1. INTRODUCTION TO THE REGIONAL GEOLOGY OF UGANDA

1.1. Geological framework of Uganda (GSD)

Geology of Uganda is composed of Lake Victoria Terrane (LVT) craton which is Neoproterozoic granite greenstone terrain comprising volcanic dominated Nyanzian Supergroup and sediment dominated Kavirondian Supergroup. The Lake Victoria Terrane also comprises a nepheline-syenite body (2.63 Ga). The West Tanzania Terrane (WTT), which is slightly older but also Neoproterozoic (2.65–2.64 Ga), granite-gneissic migmatitic terrain, is overlain by rocks of the Paleoproterozoic Rwenzori belt. Both correspond with an anomalous magnetic zone separating them from the LVT (South) and NUT (North). The West Nile Block (WNB) constitutes the Eastern, Uganda segment of the Bomu-Kibalian shield of NE Congo. The WNB comprises a Mesoarchean core (Uleppi Complex), composed of granulites (< 3.08 Ga) and associated charnockites. This core has accreted with Neoproterozoic rocks of the Arue Complex, comprising mainly amphibolite-grade supracrustals of the Lobule Group, variable gneissose granitoids (2.65 Ga), charnockites (e.g., Tera brown granite > 2.63–2.62 Ga) and extensive younger gneissose granitoids.

The North Uganda Terrane (NUT) comprises a small segment of Mesoarchean (2.99 Ga) Karuma Complex. The bulk of the NUT is composed of Neoproterozoic rocks that have been divided into supracrustals of Amuru Group and some units of igneous or uncertain derivation with ages ranging from 2.73 (Kaseeta granite) to 2.61 Ga.

The Rwenzori fold belt (RFB) comprises older (2.21–2.15 Ga) gneissose/granitoid basement, Rukungiri Suite. This is covered by metasediments and mafic, partly pillow textured, volcanics of Buganda Group (2.00–1.95 Ga) into which syn-tectonic granitoids of the Mubende-Singo Suite (1.85 Ga) have been emplaced.

Post-tectonic molasses-type sediments of the Namuwasa Group were deposited, buried and deformed between < 2.05 and > 1.85 Ga. The Bwezigoro Group was deposited after 1.97 Ga and may be 50–500 million years younger than rocks of the Namuwasa Group. Deposition of similar molasses-type deposits of Kagera-Buhweju Supergroup started at 1.79 Ga.

The North Kibaran Belt (NKB) comprises abundant S-type peraluminous granitoids. The Kabanga-Musongati mafic and ultramafic layered complex (1.40–1.38 Ga) and mafic dykes and sills, including the huge Lake Victoria arcuate dyke swarm (1.37 Ga) belong to the North Kibaran Igneous Province (1.40–1.33 Ga). The igneous rocks are more or coeval with a thick pile of metasediments of the Akanyeru-Ankole Supergroup Makitie et al. 2014.

There is newly identified N-S trending double-verging thrust and shear belt separates the WNB from NUT called Madi-Igisi Belt. It comprises stack of reworked Archen rocks of the WNB and or NUT (e.g., Yumbe duplex structure) and juvenile lithologies. The latter are assembled in the Mirian Supergroup, comprising variably metamorphic volcanics (0.98 Ga), metasediments (< 1.0 Ga) and rare ultramafics of the Madi and Igisi groups.

Deposition of the Malagarasi Supergroup started prior to 0.89 Ga and was concluded with deposition of glaciogene diamictites, resting on dated continental flood volcanics with age of 0.82–0.79 Ga. Molasse-type Mityana Group and younger to periglacial rocks of Bunyoro Group supposedly coeval with the global glaciation dated between 765 and 735 Ma.

Collision between of East and West Gondwana and their amalgamation gave rise to development of the East African Orogen, represented by the Karamoja belt in Eastern Uganda. It comprises juvenile allochthonous rocks of the Karasuk Supergroup and allochthonous rocks of the newly identified west Karamoja Group, characterized by the presence of UHT

granulites and 0.74–0.68Ga charnockites. A number of in situ Pan- African granitoid bodies of the Adjumani-Midigo Suite (0.66 Ga) are tentatively related to southward subduction of the Saharan Metacraton below Gondwana.

Karoo basins (290–180 Ma) in South Uganda are restricted to a few small occurrences. Late Eocene–Neogene rifting and development of the East African Rift System (EARS) is expressed in eastern Uganda by Elgon Complex comprising a huge pile of predominantly pyroclastic and lahar-type alkaline-sodic volcanic rocks and associate carbonatite plugs and fenites. The Albertine Rift in the west comprises relatively thick (4 km) hydrocarbon bearing sequence of terrigenous sediments (< 16 Ma) and ultrapotassic and carbonatitic volcanic rocks of Pleistocene to Holocene age.

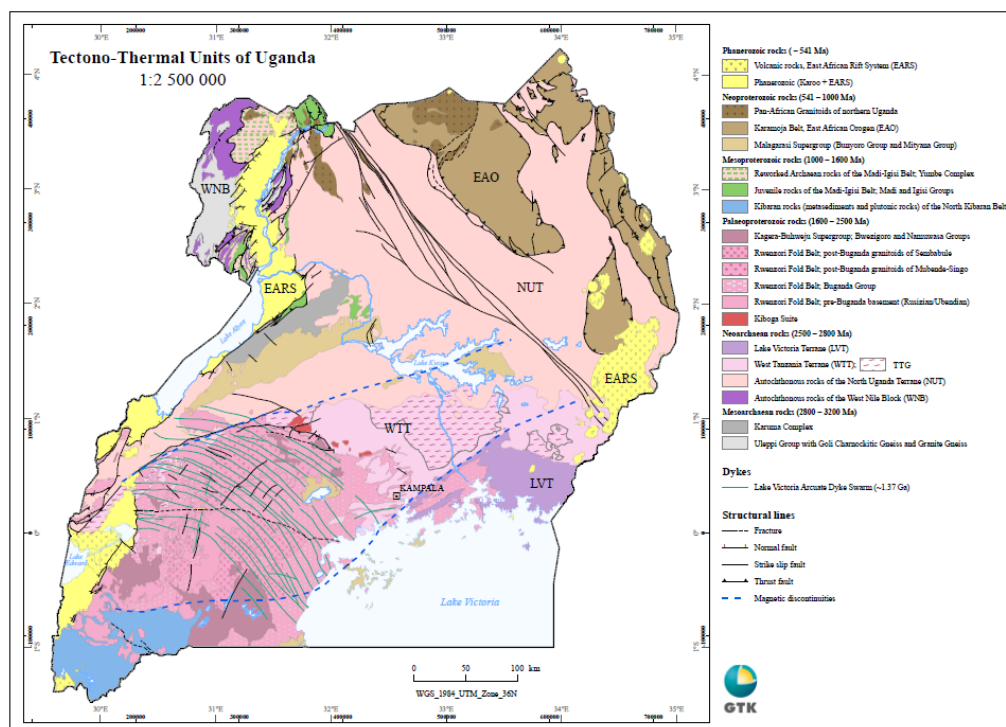


Figure 1. Geology map of Uganda.

1.2. Regional tectono-metamorphic framework of the SW part of Uganda

The Karagwe-Ankole Belt (KAB) is an orogenic belt located in Central Africa, covering the countries Rwanda and Burundi, and parts of south-western Uganda, north-western Tanzania and the former Kivu and Maniema provinces of the D.R. Congo. The KAB forms the north-western continuation of the Kibaran Belt (KIB) in the D.R. Congo and is divided along the mafic–ultramafic Kabanga-Musongati (KM) alignment in a Western Domain (WD) with Paleoproterozoic basement and an Eastern Domain (ED) with Archean basement, each representing independent sub-basin(s) (Tack et al. 1994). Sediments in these intracratonic KAB basins were deposited between 1420 Ma and 986 Ma (Fernandez-Alonso et al. 2012). Together, the Mesoproterozoic KAB and KIB were previously defined as the Kibaran Belt *sensu lato* (Tack et al. 2010). Although they show similarities in sedimentation, magmatism and deformation histories, they are structurally separated from each other by the uplifted, NW-trending Rusizi-Ubende Belt.

Multiple geodynamic models have been proposed for these two belts during the Meso- and Neoproterozoic (De Waele et al. 2008, Tack et al. 2010, Fernandez-Alonso et al. 2012).

Generally, the KAB is interpreted to have developed in the Mesoproterozoic extension–compression setting of the proto-Congo Craton that existed as one coherent entity since 1375 Ma, possibly even since 1.8 Ga (e.g., De Waele et al. 2020, Fernandez-Alonso et al. 2012, Klerkx et al. 1987, Tack et al. 2010). Other studies favour a subduction/ collision setting in the KAB during the Mesoproterozoic, as generally proposed for the KIB (e.g., Debruyne et al. 2015; Koegelenberg & Kisters 2014; Kokonyangi et al. 2005, 2004, 2006; Pohl 1988). In both scenarios, compressional deformation took place at the start of the Neoproterozoic, influenced by the distant Irumide Belt formation in Zambia and Malawi as a part of the Rodinia amalgamation (Fernandez-Alonso et al. 2012). This event was closely followed by an important granite-related mineralization in the WD of the KAB. Granite-related Nb–Ta–Sn mineralized LCT-pegmatites and W- or Sn-bearing quartz veins were emplaced in the period between 998 and 957 Ma (e.g., Dewaele et al. 2011, Hulsbosch et al. 2016, Melcher et al. 2015). This mineralization has been related to extreme fractional crystallization (pegmatites), fluid exsolution and fluid mixing (hydrothermal quartz veins) (Hulsbosch et al. 2016, 2014; Van Daele et al. 2018a). Around 550 Ma, a NS-oriented Pan-African deformational overprint was recorded in the KAB, and has been related to the East African Orogeny during the Gondwana amalgamation (Dewaele et al. 2011, Fernandez-Alonso et al. 2012). However, the external far-field character of the two Neoproterozoic deformation events (at c. 1000 and c. 550 Ma) was challenged based on the regional-scale geometry, kinematic structures and metamorphic zonation of the belt (Koegelenberg & Kisters 2014). Additionally, a Neoproterozoic metamorphic episode has been dated in the KAB at 966 ± 11 Ma (SHRIMP U–Pb age of metamorphic zircon rim; Tack et al. 2010) and 962 ± 7 Ma (U–Pb garnet in metamorphosed granite; de Kock et al. 2014).

In addition, multiple geochronological studies show disperse, mostly Neoproterozoic ages ranging from 1082 to 486 Ma (Cahen et al. 1984; Dewaele et al. 2011 – U–Pb on columbite-tantalite, Ar–Ar on muscovite; Van Daele et al. 2018b – Rb–Sr and Ar–Ar on phyllosilicates).

The area south of Karagwe-Ankole Belt first underwent a prograde Barrovian-type metamorphism with the peak metamorphism at amphibolite facies conditions (up to 630°C) during the Meso- and Early Neoproterozoic, which was followed by widespread post-deformational greenschist facies overprint ($T = 525^\circ\text{C}$ to c. 440°C) at the end of the Neoproterozoic.

1.3. Summary of geological setting of the Kabale region

This text was compiled from the Explanatory notes to the Kabale Sheet (Westerhof, Pekkala & Lehto et al. 2011), the map image from Fig. 2 also from the notes to the neighbouring sheet Mbarara.

Most of the rocks in the Kabale Map Sheet area (SA-36-5) belong to the intracratonic Mesoproterozoic North Kibaran Belt. This fold belt used to be divided into an Eastern External Domain with a succession of platform rocks (1–3 km thick) of the former foreland of the Kibaran trough, and an Eastern Internal Domain, comprising a thick pile (over 10 km in the central part of the trough) of folded, thrust and metamorphosed terrestrial sediments (Tack et al. 1994, Tahon et al. 2004, Fernandez-Alonso et al. 2006).

Mbarara (SA-36-1)

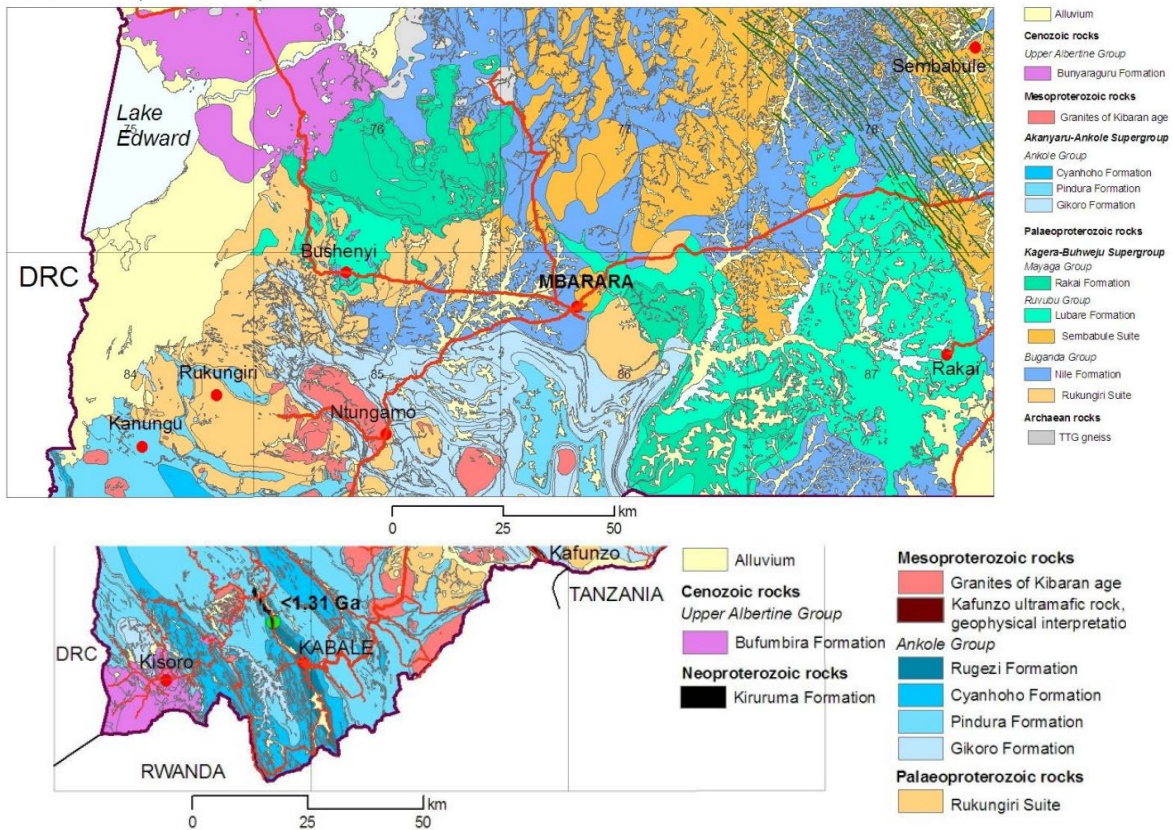


Figure 2. Simplified geological map of most part of the area between Entebbe and Kabale, covered by map sheets of Mbarara (upper) and Kabale (lower, GTK 2011)

New geochronological data, including zircon U–Pb SHRIMP dating of a tuff layer in the basal part of Kagera-Buhweju Supergroup, yielded a crystallisation age of 1780 ± 9 Ma (Cutten et al. 2004) and indicated that the alleged foreland deposits of the North Kibaran trough are some 350 million years older than the thick pile of folded, thrust and metamorphosed terrestrial sediments in the North Kibaran Belt and, consequently, cannot be longer regarded as coeval foreland deposits. The rocks of the platform sequence are therefore attributed to a separate tectono-thermal domain (Westerhof 2012) and assigned to the Kagera-Buhweju Supergroup. They do not occur in the area covered by the present Map Sheet of Kabale, but underlie extensive areas in, e.g., the Mbarara Map Sheet area to the north.

The deformed and metamorphosed sediments of the North Kibaran Belt have been attributed to the Akanyaru-Ankole Supergroup. Rhyodacite in the lower part of Akanyaru sediments in Rwanda yielded a poorly constraint WR Rb-Sr age of 1353 ± 46 Ma (Klerkx et al. 1987). The Akanyaru-Ankole sedimentary cover overlies a poorly dated basement, supposedly with a tectonic contact. This basement is composed of strongly deformed para- and orthogneisses, which are attributed to the Ruzisian in Rwanda, Burundi and Kivu (DRC) and to the Toro Complex in southwestern Uganda. Historically, the Paleoproterozoic basement has been related to the Ubende Belt of Tanzania (Cahen et al. 1984), which has been dated between 2.10 and 1.86 Ga (Lenoir et al. 1994). Rocks attributed to the Toro Complex of Uganda comprise the Rukunkiri gneiss (partly in the present Map Sheet area) dated at 2147 ± 16 Ma and the Kalonga granitic gneiss (in the Kampala Map Sheet) dated at 2.15 Ga. In Uganda, this Toro basement is overlain by undated metasediments and associated basaltic lavas of the Buganda Group. The latter have been invaded by granitoids of the Sembabule Suite (Mbarara and Kampala Map Sheets) dated at 1987 ± 5 Ma and 1964 ± 4 Ma (samples UG-19_12441 and UG-18_12404 in Mänttari 2010a). As a consequence, the age of the rocks of

the Buganda Group can be bracketed as being < 2.1 Ga and > 1.99 – 1.96 Ga. Recently, a 'Rusizian'-aged basement orthogneiss in the Butare area (south central Rwanda) has been dated and yielded a SHRIMP age of 1982 ± 6 Ma (Tack et al. 2010).

A bimodal, approximately 1.4 Ga suite of granitoids, minor felsic volcanics and mafic sills and dykes has been emplaced into the North Kibaran Belt and beyond. The event heralds a period of extension in the North Kibaran Belt culminated during a relatively short interval between 1375 and 1380 Ma with the intracratonic emplacement of a large igneous province (Tack et al. 2008, 2009, 2010) termed North Kibaran Igneous Province (NKIP) in the Explanatory notes, allegedly related to a thermal (mantle) anomaly giving rise to coeval bimodal magmatism. These include the 'Kibaran Peraluminous Granites' of Klerkx et al. (1987) and Tack et al. (1994). They have slight variation in chemical composition (Fernandez-Alonso 1981, Fernandez-Alonso et al. 1986, Fernandez-Alonso & Theunissen 1998). In an alkalinity diagram ($\text{Na}_2\text{O} + \text{K}_2\text{O}$ versus SiO_2) both types can be described as granite and alkali-granite with subordinate granodiorite and syeno-diorite. All have a calc-alkaline to slightly alkaline signature and are peraluminous.

Outside the Kabale area, this major igneous event is represented by a huge set of curvilinear sheeted dolerite dykes, attributed to the Lake Victoria Arcuate Dyke System (see Mbarara Map Sheet; SA-36-01) and layered mafic and ultramafic bodies of the 'Kabanga-Musongati-Kapalagulu Nickel Belt' in Burundi and NW Tanzania.

Emplacement of some Kibaran granitoids from southwestern Uganda apparently preceded emplacement the bimodal NKIP. The nearby Chitwe and Ntungamo batholiths show crystallisation ages of 1566 Ma and 1445 ± 8 Ma (Buchwaldt et al. 2008). Otherwise, they resemble granitoids of the NKIP in tectonic setting and composition.

The North Kibaran orogenic cycle was closed with emplacement of late syn- to post-kinematic so called 'tin granites'. These sub-outcropping granites are believed to be the parent of widespread mineralized pegmatite bodies dated at 970 Ma and quartz veins dated at 950 Ma. These Kibaran 'tin granites' and associated pegmatite bodies and quartz veins host numerous tin-tantalum-gold-tungsten-beryllium in greisen-type occurrences which are common in the SW of Uganda.

A rare occurrence of Neoproterozoic glaciogenic deposit with tillites and dropstones and an abraded bedrock surface below was observed along the slope of a wide valley: the Kiruruma Formation. This deposit is provisionally attributed to the uppermost part of the Neoproterozoic Malagarasi Supergroup.

The Kabale map sheet area includes the particularly scenic SW corner of the country, around the town of Kisoro, with a young 'volcanogenic topography' of the Virunga Mountains, on the triple junction formed by the borders of Uganda, Rwanda and Congo. Recent ash falls cover the rocky slopes underlain by Ankolean rocks. Although only a few centimeters to decimeters thick, they render these hills particularly fertile. The volcanics belong to Bufumbira Volcanic Field, one of the volcanic fields in the Albertine Rift, the northernmost part of the Western Rift of the East Africa Rift System (EARS). They are attributed to the Bufumbira Formation and comprise a variety of late Late Pliocene–Holocene explosive (ultra)potassic volcanic products.

1.4. Road geology between Entebbe and Kabale – Monday March 4, 2024

The geology varies from Entebbe to Kabale in the Buganda-Tooro system and Karagwe-Ankole/Akanyeru-Ankole belt. Buganda-Toro system consist of granite gneiss, quartzite, phyllites, slates, biotite porphyritic granite, sandstones and Akanyeru-Ankole belt mainly

comprised of porphyritic biotite granites, shales, mudstones, sandstones, siltstones, phyllites, schists and dark grey to black graphitic phyllites.

Stop at the granite outcrop along the Kabale–Mbarara Road: Weathered granite wall cut by erosional gully. Outcrop shows coarse-grained biotite granite sheared by two brittle fracture systems partially filled with quartz. Granite encloses small xenoliths of country metasedimentary rocks up to 10 cm, without any visible effect of contact metamorphism (locality U01, WGS84: 29.968° E, 1.242° S).

2. METHODOICAL EXCURSION

2.1 Outline

Methodical excursion No. 1 Geology and lithology:

Leaders: Vladimír Žáček, Zuzana Tasáryová
Localities: Nos. 1 to 5

Methodical excursion No. 2 Structural geology

Leaders: Pavel Pitra, Sudan U. Birungi
Localities: Nos. 6 to 10

Methodical excursion No. 3 Geophysics

Leaders: Nelson Birungi, Joseph Nyago
Locality: Geophysical polygon near Kabale and Polygon D

Methodical excursion No. 4 Geochemistry

Leaders: Deus Katomi, Veronika Štědrá
Localities: Road cuts along Kabale–Mbarara road, River bed near Butaare, NE from Kabale

2.2 Methodical excursion No. 1 – Geology and lithology

Locality 1. Profile in a road cut at Kakore village

(U-08, WGS84: 29.928° E, 1.171° S)

The locality offers an excellent profile in clastic sediments about 400 m long with height of 4–6 m situated along with the main road. Two geological units are exposed along the profile, which are separated from each other by a distinct hiatus. An older unit of the Mesoproterozoic Akanyaru-Ankole Supergroup (1.6 Ga) is exposed in the part of the defile closer to Kabale. It is an alternation of massive sandstones with subordinate gray siltstones to phyllites, which, in addition to the stratification form a clear anticlinal structure in the profile. The rocks are also locally affected by a noticeable metamorphic foliation. There is also a steep shear zone in these rocks in the western part of the outcrop towards Kabale. This folded and foliated unit is overlain by the subhorizontally deposited, finely laminated siltstones of the Kiruruma Formation, which contain in

some places more abundant, in other places only isolated boulders of rock 1–25 cm in size, interpreted as dropstones. The contact of the two units is approximately in the middle part of the profile (Fig.3), the discordance is noticeable at the base and lies at a 50 cm thick layer of basal conglomerates (tillites?). An abraded uppermost bedding plane of the Akanyaru-Ankole Supergroup with scratch marks could originate due to rock fragments lodged in the base of a moving glacier. Some layers are more resistant and selectively weathered. Laminated siltstones with boulders are interpreted as glaciogenic sediments – diamictites with dropstones. The age of rocks is of Neoproterozoic age, younger than c. 1.31 Ga, but they can be even deposited later, during Cryogenian at c. 700 Ma.



Figure 3. Contact between folded and foliated Akanyaru-Ankole Supergroup (left) and younger glaciogenic Kiruruma Formation of Neoproterozoic age (right).

Locality 2. Road cut in Mesoproterozoic sandstones at Hamorwa village

(U-07, WGS84: 29.905° E, 1.128° S)

This road cut is about 300 m long and 4–7 m high. Grey-white to reddish medium- to coarse-grained sandstones, laminated in red with varying intensity, are exposed here. They belong to Mesoproterozoic Akanyaru-Ankole Supergroup. The red coloring is from finely dispersed hematite. Sandstone forms beds up to 150 cm thick separating each of other by a thin intercalation of clay (Fig. 4). The dip is at medium angle toward NE. There are well-preserved primary sedimentary structures as ripple marks on primary seabed surfaces. In places, an overprint by a steep foliation parallel to the pronounced N–S trending subvertical fracture zone is visible.



Figure 4. The bedded sandstone of the Akanyaru-Ankole Supergroup (1.6 Ga), with apparent sedimentary bedding and ripple marks.

Locality 3. Road cut in Mesoproterozoic sandstones and siltstones at Kanyakwazi village

(U-29; WGS84 29.843° E, 1.183° S)

The road cut is approximately 50 m long up to 4 m high. Alternation of sandstone and laminated claystone beds, c. 20–100 cm thick, is exposed here (Fig. 5). Sandstones



Figure 5. Laminated sandy siltstones and claystones which belong to the Akanyaru-Ankole Supergroup (1.6 Ga).

are harder and selectively weathered. The sequence dips rather steeply to the NE. The sequence is a part of the Mesoproterozoic Akanyaru-Ankole Supergroup.

Locality 4. Small quarry in Mesoproterozoic granite at Hakabujara village

(U-28; WGS84 29.842° E, 1.172° S)

Exposure is cut by the road in granite, also small abandoned quarry 10 × 10 m was opened in the granite wall about 5 m high (Fig. 6). It is formed of heavily weathered, coarse-grained tourmaline muscovite granite. There are rounded blocks in the quarry representing less weathered cores of exfoliated matrix granite. Tourmaline forms either cm-sized veinlets or small irregular nodules in the granite. A turn off to an unpaved road along the creek to the North and to the tungsten mine associated with pegmatite, is across the small bridge.



Figure 6. Abandoned quarry with strongly weathered tourmaline-muscovite granite. Quartz veinlets or cm-scaled nodules with black tourmaline are also present.

Locality 5. A large quarry in Neogene volcanics at Kikombi

(U-30; WGS84: 29.847° E, 1.162° S)

Large quarry in Kikombi, or rather a sand pit, with excavated Neogene basaltic lavas and volcanoclastics for road repairs. Rocks belong to Albertine Group related to the activity of the Eastern African Rift System. The width of the quarry is about 150 m, and the height reaches 15 m. At the base of the quarry, a sharp contact of volcanics with granite is exposed. Granite is medium to coarse-grained, tourmaline-bearing with nests up to 3 cm, but heavily weathered. The entire hill above the quarry is covered with terraced fields. The field of satellite images still shows two craters several hundred meters in diameter, which form shallow circular depressions today. In the exposed part, two principal layers are visible, from the base up to about 10 m of coarser pyroclastic rocks, and above them a sharply separated position of lapilli accumulation (Fig. 7). The lower layer of coarse pyroclastic fall deposits contains cm- to meter-sized volcanic bombs or discontinuous lava flows with blocks up to 150 cm in size. The lava is massive, locally very porous, with up to several centimeters of cavities due to escaped gases (= vesicles). Volcanic bombs up to several dm in size are common.

Up to 1 cm crystals of dark pyroxene, greenish glassy olivine and cleaved colorless sanidine are visible in the lava. Rarely, there are white porous aggregates resembling pumice. They are probably molten xenoliths of the underlying granite. The coarse-grained pyroclastic rocks are overlain by a layer of loose layered lapilli fall deposits with clasts of mm to several cm size.

Phenocrysts of pyroxene, olivine, and K-feldspar (sanidine) were identified in the thin section, and there is similar material in the matrix, plus a small amount of fine-grained anhedral nepheline. The rock is a basic alkaline effusive rock related to rift and corresponds to basanite.



Figure 7. Part of the profile in the Kikombi quarry. The coarse-grained pyroclastic fall deposits are overlain by a layer of loose layered lapilli with clasts of mm to several cm size (above). Layered accumulations of lapilli (left). Volcanic bomb with heterogeneous composition and structure (right).

2.3 Methodical Excursion No. 2 – Structural Geology

Locality 6. Gravel quarry in sandstone, Kidzuguta near Kabale

(U-02, WGS84: 1.2390° S, 29.9675° E)

Along to road to Kisoro, about 3 km NW of Kabale, a number of quarries or occasional quarries of various sizes display layers or beds of sandstones with intercalations of soft clayey or silty grey shale. Hard sandstone is mined for gravel in these quarries.

The visited quarry is about 35 m wide; the wall is up to 10 m high (Fig. 8a). Local small-scale miners manually mine and crush the material into gravel. The exposed rock is dominantly a fine- to coarse-grained, locally very hard sandstone to conglomerate forming beds 0.5–2 m thick. The sediments belong to the Mesoproterozoic Akanyaru-Ankole Supergroup. The individual sandstone beds are separated from one another by laminae of more fine-grained, clay-like material. Sandstones have a reddish hue due to finely dispersed hematite. Conglomerates contain rounded to subangular, mostly flat, disk-shaped clasts of whitish-yellowish fine-grained rock (Fig. 8c) that locally contains white-mica and displays fine layering. It is either a clayey shale or a felsic volcanic rock or tuff. One bed a very heterogeneous conglomerate is present in the bottom of the quarry. It contains rounded clasts of felsic coarse-grained material (possibly a granitoid) up to 15 cm in size (Fig. 8d). The bedding dips at an angle of 30–45° to the SW (Fig. 8b). The rocks are cut by several sets of fractures. Several listric faults, containing tectonic breccia up to 20 cm wide, are visible in the quarry. Under the microscope, the sandstone is composed of rounded grains of quartz and minor grains completely replaced by sericite, probably originally feldspars. The matrix is subordinate, composed of finely dispersed hematite and sericite.

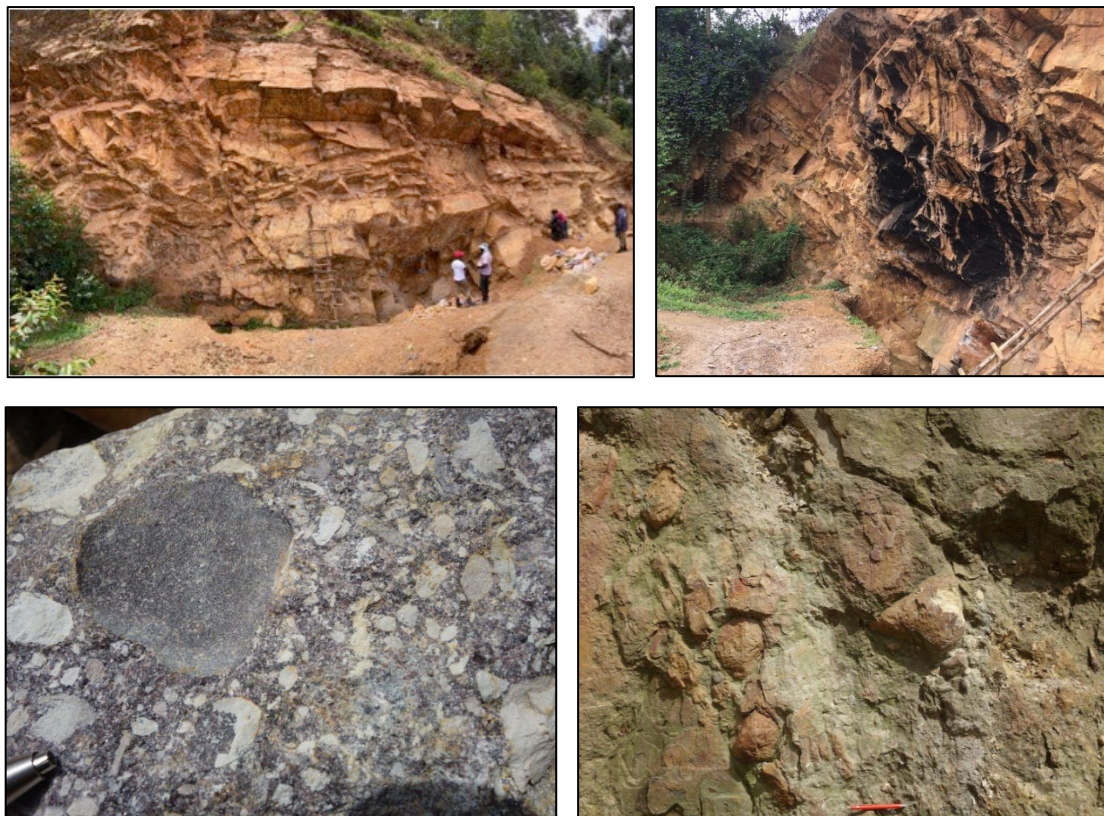


Figure 8. Sandstone quarry. a) General view. b) Looking SE: sandstone beds dip moderately to the SW. c) Conglomerate with abundant disk-shaped, light-colored clasts. d) Coarse heterogeneous conglomerate containing rounded clasts, up to 15 cm, of felsic – possibly granitic – material (note white trace after hammering on the clast in the middle).

Locality 7. Road cut c. 8 km ENE of Kabale, at a small local-farmer market

(WGS84: 1.2295° S, 30.0558° E)

Grey fine-grained muscovite-bearing slates outcrop on both sides of the road. The grain size and mineralogy suggest that they result from low-grade metamorphism of a pelitic sediment (shale). A penetrative slaty cleavage dips 55–80° to the ENE. The SE side of the road displays

a well visible bedding that is affected by gentle to tight folds (Fig. 9a). The cleavage develops in the axial plane of these folds (Fig. 9a, b). The rocks are affected by faults that juxtapose variably folded blocks (Fig. 9a, c).

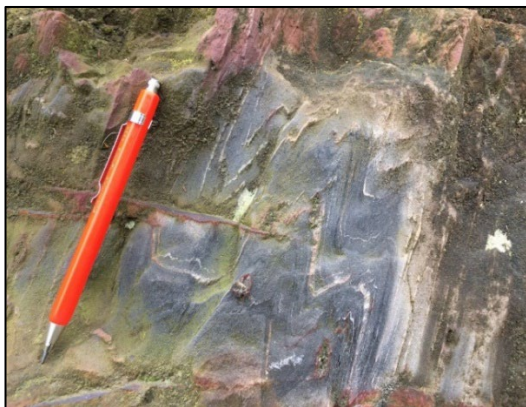
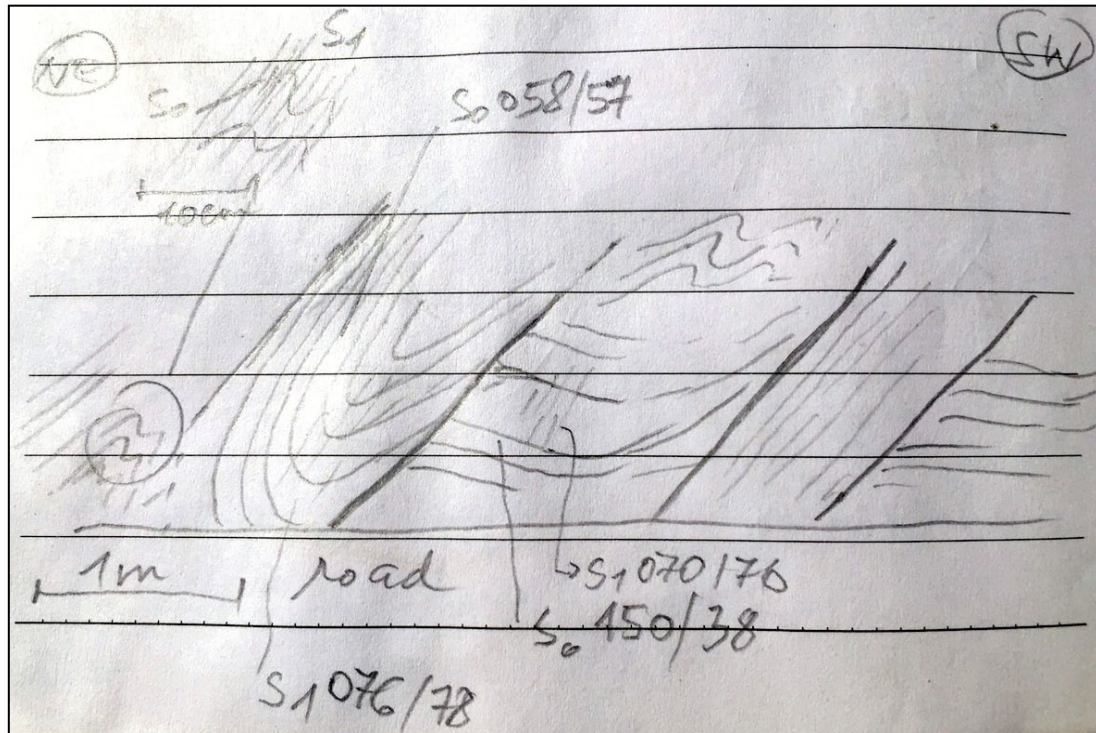


Figure 9. a) Sketch of the outcrop showing variably folded blocks separated by discrete faults, © P.Pitra. b) Detail of a dm-sized fold with axial-planar cleavage (parallel to the pencil). c) Fault (red) separating a block with a bedding (S_0 , orange) affected by a tight metric fold (left) from a block (right) where bedding (orange) gently dips to the right. The slaty cleavage (S_1 , blue) is parallel to the axial plane of the fold. All pictures are oriented NE–SW.

Locality 8. Road cut in a mountain pass, Kybugombe, c. 14 km ENE of Kabale

(WGS84: 1.2321° S, 30.1128° E)

The hundred-meters long roadcut exposes a sequence of grey fine-grained slates interlayered with cm–dm thick beds of coarser-grained white sandstone. Sedimentary structures are

beautifully preserved in the sandstone on the eastern side of the road. They include ripple marks and cross-bedding (Fig. 10a). The fine-grained grey layers display a cleavage. On the western side of the road the sequence of slates and sandstone is affected by an overturned fold, where the axial-planar cleavage developing convergent and divergent fans can be observed (Fig. 10b).



Figure 10. a) Ripple marks and cross-bedding in white sandstones interlayered with grey slates. The image is oriented N–S. b)

The slate-sandstone sequence is affected by an overturned fold (pencil, c. 10 cm long, for scale). The axial planar cleavage is dipping dipping to the right (east). c) Detail of the hinge zone of the fold, displaying divergent axial-planar cleavage fans in the slate layers (point of a pencil for scale). Orientation: W–E.



Locality 9. Abandoned granite quarry at Kabira, c. 19 km NE of Kabale

(U-18, WGS84: 1.1557° S, 30.1305° E)

Large abandoned granite quarry by the road Kabale–Mbarara, c. 200 m wide and a wall height of up to approx. 25 m. Several types of granite are exposed here. Right next to the eastern wall, a zone of quartz vein up to 30 cm thick penetrates the granite in an approximately E–W direction. Grey coarsely porphyritic biotitic granite occurs near its eastern and central parts of the quarry, whereas a light grey fine-grained granite to leucogranite dominates the western part. They are cut across by three, dominant orthogonal sets of joints. In places, the granite is weathered to coarse sandy grit. Decimeters long veins of barren pegmatites, occasionally with nests of black tourmaline up to 5 cm, break through the granite in several domains. In the western part of the wall, the granite is deeply weathered into eluvium. In the western edge of

the quarry, a large amount of red laterite is sliding from the upper part of the wall and is excavated by local people for construction material.

2.4 Geophysical survey methods practice

2.4.1. Aim of the survey

The aim of the survey is to introduce and demonstrate to the field participants the aspects of magnetic survey planning, data acquisition procedures and practices involved in the execution of a ground magnetic data acquisition, processing and interpretation.

2.4.2. Survey area

The survey area is within polygon 'D' located near Kacherere trading centre in Rubaare Sub County, Ntungamo district which is about 45 minutes' drive from Kabale town towards Ntungamo town. The choice of the survey area for this field demonstration was chosen based on the terrain of the area since the rest of the polygons were characterized by bad terrain. A total of 8 profiles, each of approximately 800 meters long were surveyed during the 4 days the team spent out in the field, with an approximate profile spacing of 200 meters (Figs. 11, 12). Each group was handling two (2) profiles per day.

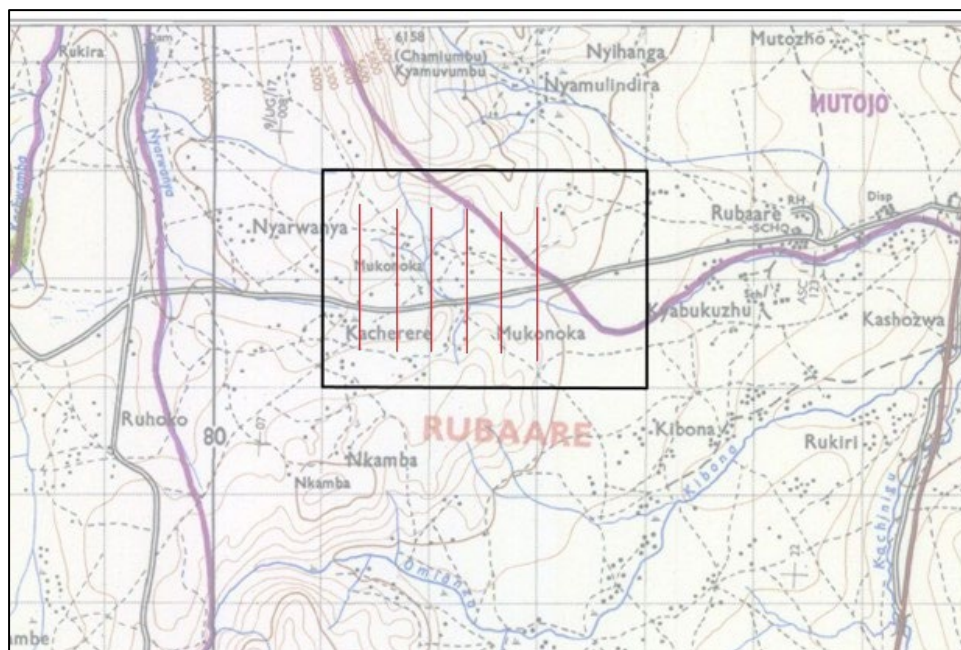


Figure 11. Topographic sheet map of the Polygon D area showing the planned traverse lines.



Figure 12. Google Earth image of the area and the planned survey traverses.

2.4.3. Methodology

Gravity, Magnetics and Radiometry have been carried out along parallel grid lines of constant spacing.

The grid lines and station spacings are designed in such a way that the Fourier wavelengths of the smallest recoverable anomalies being sought are appropriate to the design. The survey traverses are planned by making use of Google Earth, topographic maps in consideration of existing geological maps. This was done to ensure delineation of possible geological structures (e.g., dykes). The base stations for gravity, magnetics and the differential GPS were maintained at the same spots for all the transects. The traverse lines and way points were uploaded to hand-held GPS. The magnetometer rover and base station had both GPS which stream the location of each data point in real-time. The data collection interval for the base station and rover were set at 0.5 seconds. This ensured that enough data points were collected for data reduction.

Gravity measurements were acquired at 50 meters station interval with a sampling rate of 6 Hz averaged over 60 seconds to suppress seismic noise. while radiometric measurements were taken in survey mode with a Bluetooth GPS, where the total count read is between 1–20 second integration rate along the same profiles.

2.4.4. Survey design

The traverse and line spacing were designed using Geosoft and all the planned traverse was finalized using ArcGIS (see Fig. 13). The following survey parameters were used in this study; traverse direction was N–S, line spacing at approximately 100 m. The figure below is an example of traverse lines designed a Google Earth image of Polygon D. These traverses can also be overlain on any other maps, e.g. airborne geophysical maps.

2.4.5. Field

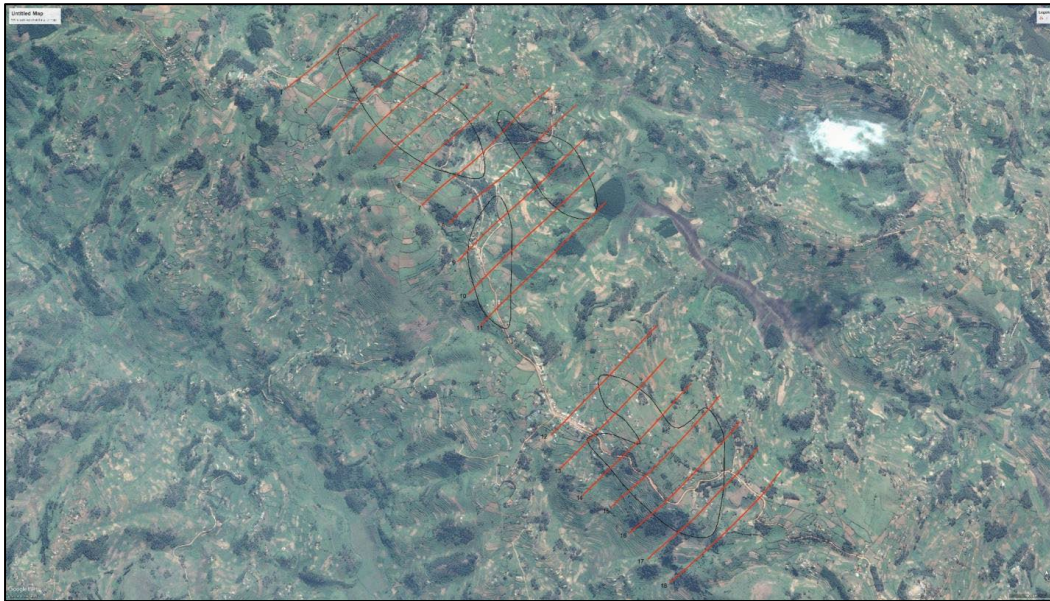


Figure 13. Ground magnetics survey plan overlain on geology and Google Earth images near Polygon B.

Magnetic data Acquisition

Several checks would always be conducted before the field survey is launched such as the instrument battery being fully charged, traverse lines designed, clearing memory of previous data as well as setting the new date and time (as explained in standard operation procedure, SOP's; Fig. 14). For magnetics, it is important to note all metallic objects e.g., bridges, near or along traverse lines as these present as noisy artefacts in the data. Geological and geophysical rock properties observations were made on the traverse lines using SM20 magnetic susceptibility meter. The data was acquired close to the ground level by a person carrying a magnetometer sensor placed at an average 3-meter height (Fig. 15). To initiate the survey, a constant point called a base station was identified for continuous data capture.



Figure 14. Field demonstration on how to set-up magnetometers for a magnetic survey.



Figure 15. Susceptibility and magnetic field data measurements along one of the traverses.

Thereafter, measurements were taken along the traverse lines using the roving segment of the setup in the walk mode of the magnetometer (i.e., measuring continuously along the line). The data from the base station served as a control point for temporal changes in the magnetic field, which was subtracted from the measured survey data. The magnetometer height was maintained. The rover data was downloaded to the laptop using GEMlink Software in XYZ format and the data was corrected for diurnal variations.

Gravity data acquisition



Figure 16. Levelling the gravimeter on its stand.

Just like it has been mentioned above in the magnetic method, checks for battery levels, available memory, instrument set-up parameters etc., are also carried out for gravity or for any other technique. A gravity base station with a known coordinate and gravity absolute value is occupied at the start of the survey to *open the loop*. This known position can be secured by a Inad marking which is permanent or in places like government owned land where development is not envisioned in the near future. The landmark should be clearly labelled for easy identification for future use. A reading is taken employing many cycles in order to get one constant value for a number of consecutive cycles (Fig. 16). The gravity readings are Qc'ed using the standard deviation (≤ 0.02) and the tilt x and tilt y values being between ± 10 . Once a value is settled upon, then the gravity meter can be transferred to the field to take gravity measurements. A DGPS base station may be set

up in the field or a Cors or SBAS network may be used. There are a variety of techniques to obtain accurate elevations using the DGPS but none of them involves using a hand-held GPS. It has a very poor accuracy for elevations.

DGPS readings are taken at every gravity station. Some stations may be repeated in the field to check the drift of the instrument. A measurement should also be repeated during the day at the base station depending on the feasibility e.g., distance to the base. At the end of the day, the loop is closed by taking a reading at the base the same way it was taken during the opening of the loop. Without closing the loop, the gravity data **CANNOT** be corrected! The gravity data from the meter is dumped onto a PC while the DGPS data is post-processed or directly used if real-time kinematic measurements were used. The coordinates of each point are tagged to the corresponding gravity data and further processing is then done.

Radiometric data acquisition



Figure 17. Google Satellite image showing the Mwerasandu tin mine and the RS-125 track around the mine crossing the main reef.

A gamma ray spectrometer is used to measure activity concentrations of gamma-emitting radionuclides of Potassium-40, Uranium-238 and Thorium-232. The equipment is light and portable and weighs about 2 kg including batteries (Fig. 20). Before the beginning of the survey, the date and time are set in the equipment so that the data is easy to find by date during the download process. The radiometric survey was carried out along the same profiles as the magnetic and gravity data acquisition. The spectrometers measure potassium in (%), equivalent uranium (eU) in ppm (Fig. 19), and equivalent thorium (eTh) in ppm because they are the only radioelements with sufficient energies that can be detected by the RS 125 NAI spectrometer. The dose rate is measured in nano Grays per hour (nGy/h) or nano Sieverts per hour (nSv/h) depending on the operator's preference. Grays are an old unit. Most people prefer Sieverts. The spectrometer was operated in survey mode where a bluetooth gps was connected to it as it took continuous measurements on the line. The spectrometer can also be operated in Assay mode where one can measure particular spots without continuous recording

(Fig. 18). The data is then downloaded using Georadis or RSAnalyst software and the various spectra can be analysed.



Figure 18. Gamma-ray spectrometry measurement in Assay mode

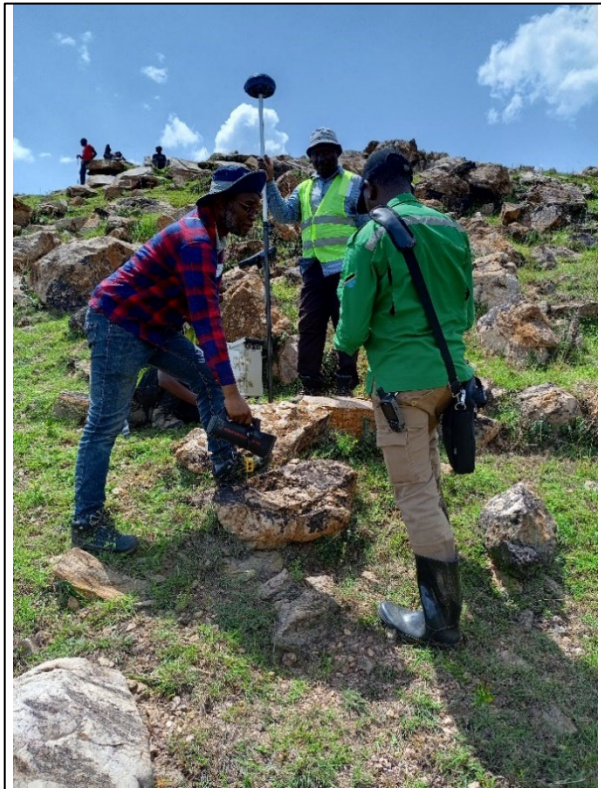


Figure 19. A 1024 channel gamma ray spectrometer reading eU more than $3 \times eTh$ around schists.

2.4.6. Geophysical data processing

Magnetics

The data from the base magnetometer served as a control point for temporal variations in the magnetic field. The base field readings are always subtracted from the measured (observed) survey data to obtain the corrected values, the process is referred to as *Diurnal Correction*. This is mathematically illustrated as follows;

$$\text{Corrected Value (nT)} = \text{Rover Field (nT)} - \text{Base Field (nT)} + \text{Datum (nT)}$$



Figure 20. In-situ gamma-ray spectrometer 1.

At the end of every survey day, the data was downloaded to the laptop using GEMLink Version 5.3 Software. The same software was used for diurnal correction which allows for input of both rover field and base field readings so as to obtain corrected readings in XYZ format for input into Geosoft Oasis Montaj for further interpretation and generation of visual images. In this field exercise, one of the magnetometer units suffered a glitch that rendered it impossible to download data off the unit. As such, the manufacturer recommended sending the unit back to the factory for troubleshooting. Therefore, a replacement dataset from Muko, an area near Polygon B has been used (Figs. 21 and 22) only for illustrative purposes of a probable outcome of a magnetic survey. Hence this dataset cannot be used in a combined interpretation with gravity & radiometric data of Polygon D, which was of interest in this exercise.

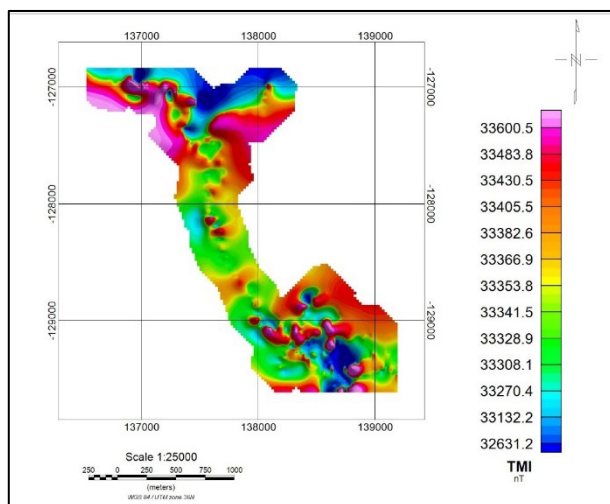


Figure 21. Total magnetic intensity map of Muko Area.

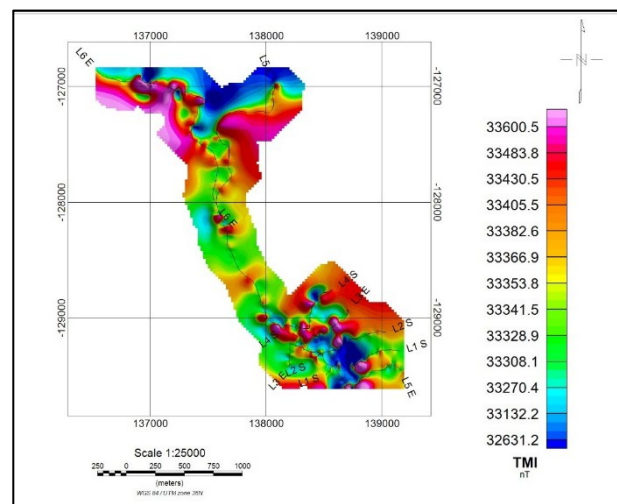


Figure 22. Total magnetic intensity map of traverses across iron ore occurrences in Muko area near Polygon B.

```
base - Notepad
File Edit Format View Help

/Gem Systems GSM-19TW 4066595 v7.0 27 XI 2014 M t-ew31.v7o
/ID 1 file 01survey.b 05 III24
/datum 57000.00
/-001.2347660 030.0625840
/UTC+03
/GPS datum WGS84

/time nT sq
132618.0 32922.88 99
132622.0 32914.12 99
132626.0 32925.21 98
132630.0 32930.09 99
132634.0 32940.81 99
132638.0 32927.57 99
132642.0 32930.78 99
132646.0 32913.25 99
132650.0 32895.79 99
132654.0 32885.45 99
132658.0 32880.00 99
132702.0 32878.10 99
132706.0 32883.98 99
132710.0 32885.09 99
132714.0 32891.43 99
132718.0 32884.90 59
132722.0 32868.18 99
132726.0 32876.49 99
132730.0 32972.34 59
132734.0 32903.35 99
132738.0 32903.05 99
132742.0 32878.00 99
```

```
03survey_wmag - Notepad
File Edit Format View Help

/Gem Systems GSM-19TW 4066595 v7.0 27 XI 2014 M t-ew31.v7o
/ID 1 file 03survey.wm 06 III24
/UTC+03
/GPS datum WGS84

/X Y elevation nT sq cor-nT sat time picket-x picket-y
line 000000
-001.0269330 030.1394172 001556 33023.38 68 000000.00 12 S 135609.0 0 0
-001.0269331 030.1394172 001556 33000.37 79 000000.00 09 S 135610.0 * *
-001.0269330 030.1394170 001556 32990.58 99 000000.00 12 S 135611.0 * *
-001.0269332 030.1394170 001556 32994.99 99 000000.00 12 S 135612.0 * *
-001.0269332 030.1394169 001556 32919.10 99 000000.00 11 S 135613.0 * *
-001.0269329 030.1394171 001556 32978.78 99 000000.00 11 S 135614.0 * *
-001.0269333 030.1394170 001556 32980.43 29 000000.00 11 S 135615.0 * *
-001.0269334 030.1394162 001556 33023.95 99 000000.00 11 S 135616.0 * *
-001.0269337 030.1394162 001557 33027.12 99 000000.00 12 S 135617.0 * *
-001.0269335 030.1394164 001557 33026.24 99 000000.00 12 S 135618.0 * *
-001.0269333 030.1394160 001557 33025.67 99 000000.00 12 S 135619.0 * *
-001.0269338 030.1394162 001557 33027.22 99 000000.00 12 S 135620.0 * *
-001.0269334 030.1394158 001557 33028.07 99 000000.00 12 S 135621.0 * *
-001.0269332 030.1394159 001557 33026.51 99 000000.00 12 S 135622.0 * *
-001.0269333 030.1394157 001557 33029.09 99 000000.00 12 S 135623.0 * *
-001.0269334 030.1394156 001557 33031.30 98 000000.00 12 S 135624.0 * *
-001.0269335 030.1394155 001557 33031.87 98 000000.00 12 S 135625.0 * *
-001.0269337 030.1394155 001557 33032.58 99 000000.00 12 S 135626.0 * *
-001.0269338 030.1394156 001557 33034.87 99 000000.00 12 S 135627.0 * *
-001.0269338 030.1394157 001557 33030.91 99 000000.00 12 S 135628.0 * *
-001.0269329 030.1394163 001557 33024.12 99 000000.00 12 S 135629.0 * *
-001.0269333 030.1394160 001557 33032.86 98 000000.00 12 S 135630.0 * *
-001.0269340 030.1394157 001557 33028.21 99 000000.00 12 S 135631.0 * *
-001.0269322 030.1394158 001557 33017.99 98 000000.00 12 S 135632.0 * *
```

Figure 23. (cont.) Examples of raw magnetic data files. (c) A typical example of diurnal corrected magnetic field data file.

```

corrected - Notepad
File Edit Format View Help

/Gem Systems GSM-19TW 4066594 v7.0 27 XI 2014 M t-ew31.v7o
/ID 14 file 01survey.wm 10 II 22
/UTC+03
/GPS datum WGS84

/X Y elevation nT sq cor-nT sat time picket-x picket-y
33452.70 i--- -001.2341805 029.6298381 001961 33150.66 99 000000.00 06 S 114546.0 * *
33452.18 i--- -001.2341810 029.6298374 001961 33150.11 99 000000.00 06 S 114548.0 * *
33451.79 i--- -001.2341817 029.6298370 001961 33149.70 99 000000.00 06 S 114550.0 * *
33451.64 i--- -001.2341821 029.6298366 001961 33149.39 99 000000.00 06 S 114552.0 * *
33453.61 i--- -001.2341831 029.6298357 001961 33151.41 99 000000.00 06 S 114554.0 * *
33448.19 i--- -001.2341846 029.6298334 001962 33146.11 99 000000.00 06 S 114556.0 * *
33445.44 i--- -001.2341881 029.6298272 001961 33143.19 99 000000.00 05 S 114558.0 * *
33445.85 i--- -001.2341896 029.6298279 001961 33143.61 99 000000.00 04 S 114600.0 * *
33448.41 i--- -001.2341890 029.6298319 001961 33146.17 99 000000.00 04 S 114602.0 * *
33459.66 i--- -001.2341822 029.6298348 001961 33157.43 99 000000.00 03 P 114604.0 * *
33496.50 i--- -001.2341719 029.6298387 001960 33194.28 99 000000.00 03 P 114606.0 * *
33516.15 i--- -001.2341697 029.6298519 001960 33213.87 99 000000.00 03 P 114608.0 * *
33486.35 i--- -001.2341711 029.6298653 001960 33184.03 99 000000.00 03 P 114610.0 * *
33521.26 i--- -001.2341695 029.6298808 001962 33218.85 99 000000.00 03 P 114612.0 * *
33520.26 i--- -001.2341666 029.6298843 001962 33218.07 99 000000.00 02 P 114614.0 * *
33526.86 i--- -001.2341635 029.6298932 001962 33224.41 99 000000.00 00 P 114616.0 * *
33543.16 i--- -001.2341605 029.6299071 001963 33240.79 99 000000.00 00 P 114618.0 * *
33524.98 i--- -001.2341575 029.6299210 001963 33222.38 99 000000.00 00 P 114620.0 * *
33491.89 i--- -001.2341546 029.6299349 001964 33189.40 99 000000.00 00 P 114622.0 * *
33490.18 i--- -001.2341516 029.6299488 001964 33187.80 99 000000.00 00 P 114624.0 * *

```

Figure 23. (cont.) Examples of raw magnetic data files. (c) A typical example of diurnal corrected magnetic field data file.

Gravity

When the gravity data has been dumped from the meter, it is subjected to further processes of reducing it to a common datum using Oasis Montaj (Geosoft) or any other suitable software. Examples of corrections applied to the data include drift, Tidal, latitude, free-air, Bouguer, elevation, terrain e.t.c. These corrections can also be done using Excel, but it is quite involving and it is easy to make a mistake in one correction that can be carried forward in all the others. An absolute gravity value of 977604.235875114 was used for the gravity base station. The gravity base station was located at Cepha's Inn.

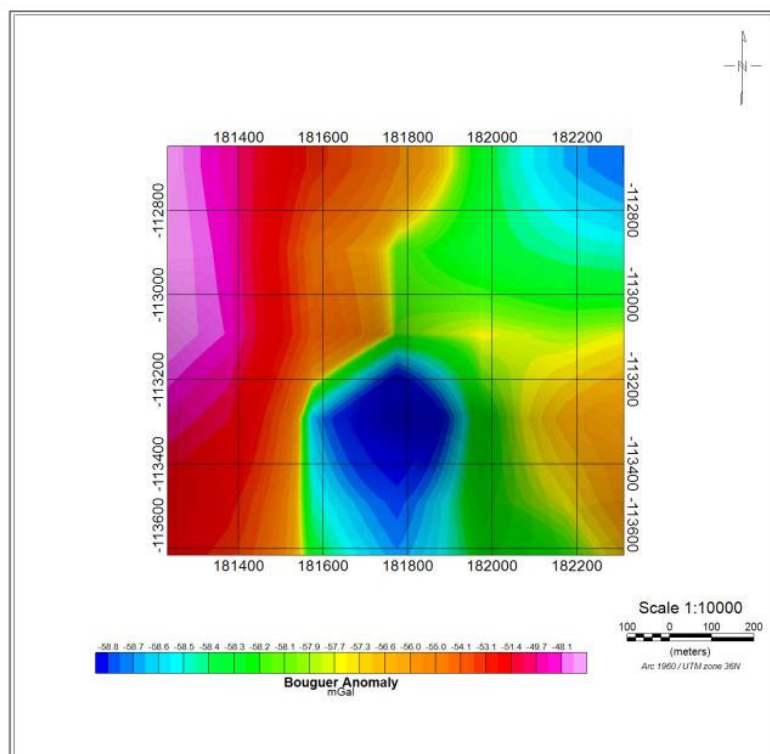


Figure 24. Bouguer Gravity Anomaly Map of Polygon D.

When all the corrections to the data are made, the columns of interest, e.g., free-air anomaly or Bouguer anomaly can be gridded for interpretation. From the gravity database, many more maps can be created, e.g., derivative maps for interpretation purposes (Fig. 24).

The data may also be modelled in 2D/3D to further aid interpretation. The process of interpretation necessitates putting together all available data, e.g., geology, geochemistry, drill core data, petrophysics, and any other available geophysical data in order to deduce meaningful products.

Radiometrics

After the data has been collected by RS-125 spectrometer, the spectrometer is connected to the PC and the RSAnalyst program started. The program opens a calendar (Fig. 25) with blue shaded dates showing that data exists on those days. Pink shaded dates are Sundays. The program, through the File Menu, allows you to create a local database where data can be downloaded to your PC. When the data has been downloaded, the spectra can be viewed (Fig. 26).

The data are then saved in CSV format which are then imported to Oasis Montaj software or any other gridding program for further processing (Fig. 27). In this case we have used minimum curvature gridding. Many more maps can be created since each map may show different facets of what is being sought.



Figure 25. RS Analyst program for radiometric data visualization.

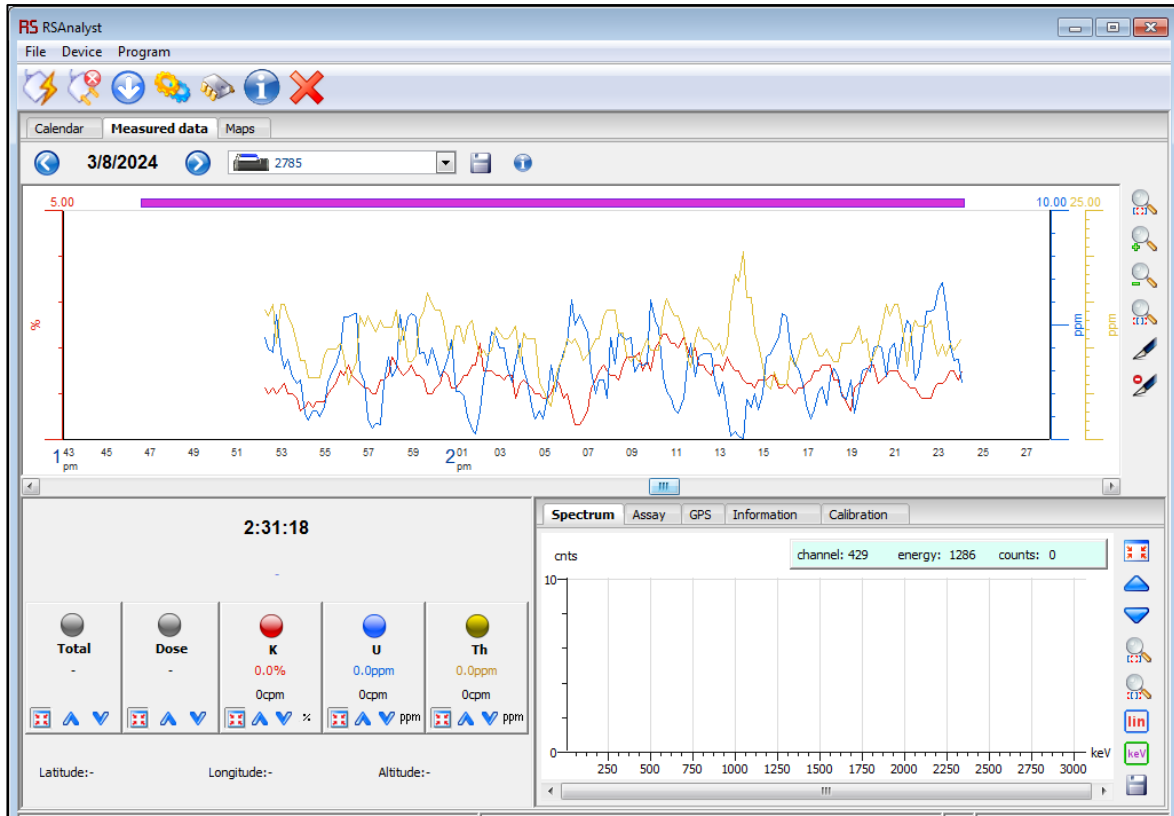


Figure 26. Recorded spectra for K, U and Th around the Mwerasandu mine.

#	A	B	C	D	E	F	G	H	I	J	K	L	M	N	O	P	Q	R
Id	Date	Time	Temperatu	Stabilized	Total[ppm]	Total[cpm]	K[%]	K[cpm]	U[ppm]	U[cpm]	Th[ppm]	Th[cpm]	Dose	units	Latitude	Longitude	Altitude	
2	44276	07/03/2024	00:00:03	30.8	1	9.7	1402	0.9	72.6	2.7	21.9	6.7	11.4	53.8 nSv/h	-1.020098	30.148507	1601	
3	44277	07/03/2024	00:00:14	30.8	1	9.4	1363.4	1	75.8	2.2	17.7	5.4	9.3	48.7 nSv/h	-1.020098	30.148508	1601	
4	44278	07/03/2024	00:00:25	30.8	1	9.7	1394.9	1	74.7	2.3	19.8	6.7	11.4	52.3 nSv/h	-1.020162	30.148537	1601	
5	44279	07/03/2024	00:00:35	30.6	1	10.3	1485	1.1	74.7	1.9	15.6	4.8	8.3	45.4 nSv/h	-1.020325	30.148577	1601	
6	44280	07/03/2024	00:00:46	30.8	1	11.4	1639.8	1	75.8	2.4	21.9	7.9	13.5	56.6 nSv/h	-1.020332	30.148617	1601	
7	44281	07/03/2024	00:00:57	30.6	1	12.6	1816.8	1.2	98.8	3.4	28.1	9.1	15.6	71.6 nSv/h	-1.020428	30.148632	1599	
8	44282	07/03/2024	00:01:08	30.6	1	13.7	1983.3	1.6	119.8	3.6	32.4	11.6	19.8	85.8 nSv/h	-1.020503	30.148633	1599	
9	44283	07/03/2024	00:01:19	30.8	1	14.4	2072.5	1.6	120.9	4.1	32.4	9.7	16.7	83.4 nSv/h	-1.020603	30.148662	1597	
10	44284	07/03/2024	00:01:30	30.8	1	13.7	1982.3	1.5	118.8	4.3	32.4	9.1	15.6	81.9 nSv/h	-1.020677	30.148698	1594	
11	44285	07/03/2024	00:01:41	30.6	1	13.1	1884.8	1.5	113.5	2.7	28.2	11.6	19.8	79.6 nSv/h	-1.020742	30.148728	1592	
12	44286	07/03/2024	00:01:52	30.6	1	12.3	1771.7	1.6	114.6	3.3	26.1	7.9	13.5	72.4 nSv/h	-1.02078	30.148777	1590	
13	44287	07/03/2024	00:02:02	30.7	1	11.6	1672.1	1.7	112.4	2.4	20.8	7.3	12.5	65.6 nSv/h	-1.020817	30.148802	1589	
14	44288	07/03/2024	00:02:14	30.7	1	10.8	1564.3	1.6	106.2	2.4	18.7	5.4	9.3	58.9 nSv/h	-1.020833	30.148853	1589	
15	44289	07/03/2024	00:02:24	30.7	1	10.7	1539.2	1.6	104.1	1.5	17.7	7.9	13.5	60.8 nSv/h	-1.020897	30.14891	1586	
16	44290	07/03/2024	00:02:35	30.7	1	10.9	1567.5	1.4	96.8	1.5	20.8	10.4	17.7	65.3 nSv/h	-1.02094	30.148908	1586	
17	44291	07/03/2024	00:02:46	30.7	1	10.8	1561.3	1.3	97.8	2.8	27.1	10.4	17.7	72.1 nSv/h	-1.020947	30.148998	1586	
18	44292	07/03/2024	00:02:57	30.7	1	10.7	1548.8	1.2	99.9	2.9	29.2	11.6	19.8	76.6 nSv/h	-1.020943	30.148998	1584	
19	44293	07/03/2024	00:03:08	30.7	1	10.8	1560.3	1.3	104.1	2.4	30.3	14.1	24	82.5 nSv/h	-1.020952	30.148882	1582	
20	44294	07/03/2024	00:03:19	30.6	1	10.7	1542.3	1.4	105.1	2.7	28.2	11.6	19.8	77.1 nSv/h	-1.02095	30.148875	1584	
21	44295	07/03/2024	00:03:30	30.6	1	10.3	1492.1	1.4	104.1	2.6	27.1	11	18.8	74.8 nSv/h	-1.020948	30.148873	1586	
22	44296	07/03/2024	00:03:41	30.6	1	10.6	1524.5	1.3	105.1	3.6	29.2	9.1	15.6	74.6 nSv/h	-1.020945	30.148872	1587	
23	44297	07/03/2024	00:03:51	30.6	1	10.7	1538	1.4	103	3.1	25	7.9	13.5	67.9 nSv/h	-1.02094	30.148873	1587	
24	44298	07/03/2024	00:04:03	30.6	1	10.7	1541.1	1.3	97.8	2.3	22.9	9.1	15.6	66 nSv/h	-1.020943	30.148877	1585	
25	44299	07/03/2024	00:04:14	30.4	1	10.3	1490.9	1	86.3	3.4	28.2	9.1	15.6	67.9 nSv/h	-1.02094	30.148868	1587	
26	44300	07/03/2024	00:04:24	30.4	1	10.5	1510.8	1.2	92.6	2.3	24	9.8	16.7	66.4 nSv/h	-1.020938	30.148875	1591	

Figure 27. Example of spectrometer record that would be exported to a gridding program.

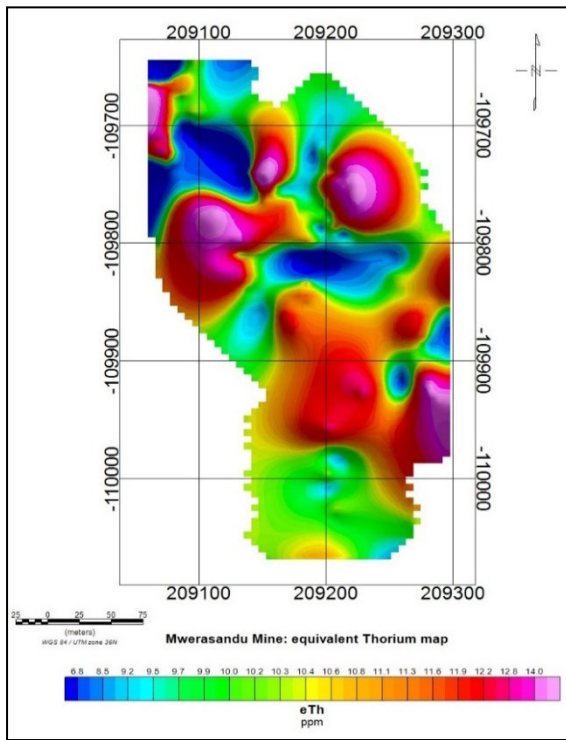
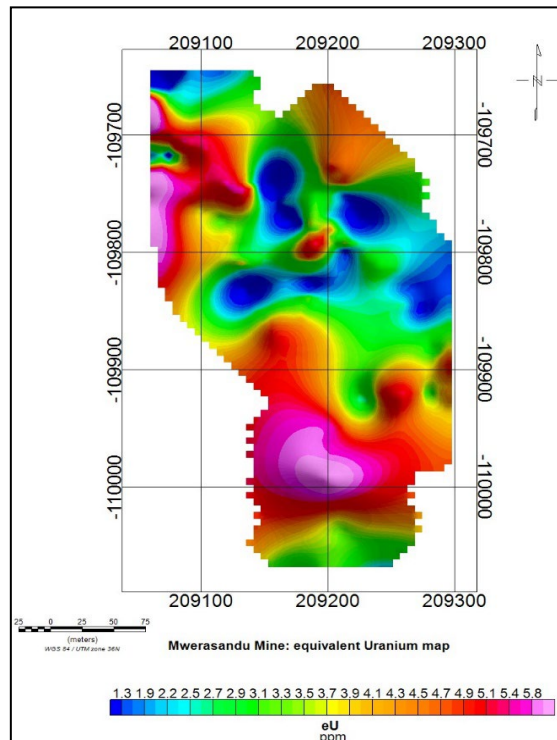
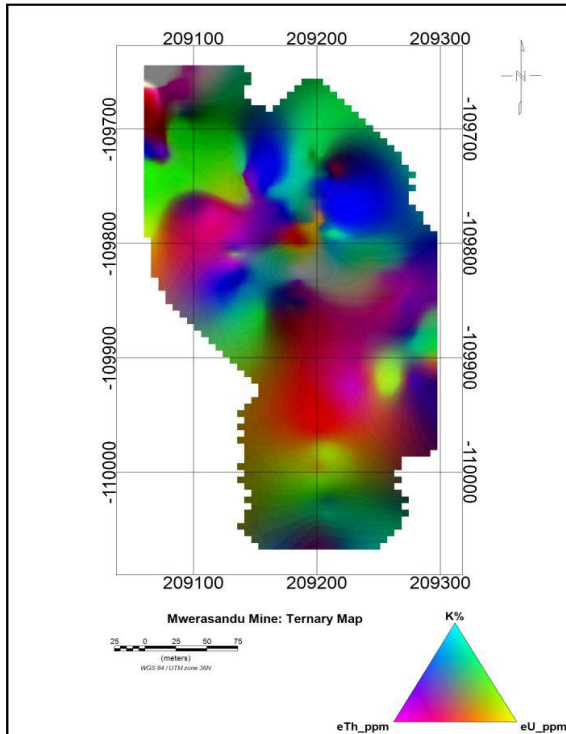


Figure 28 (a) Mwerasandu tin mine: Equivalent Uranium (eU) map.



(b) Mwerasandu tin mine: equivalent Thorium (eTh) map.



(c) Ternary image.

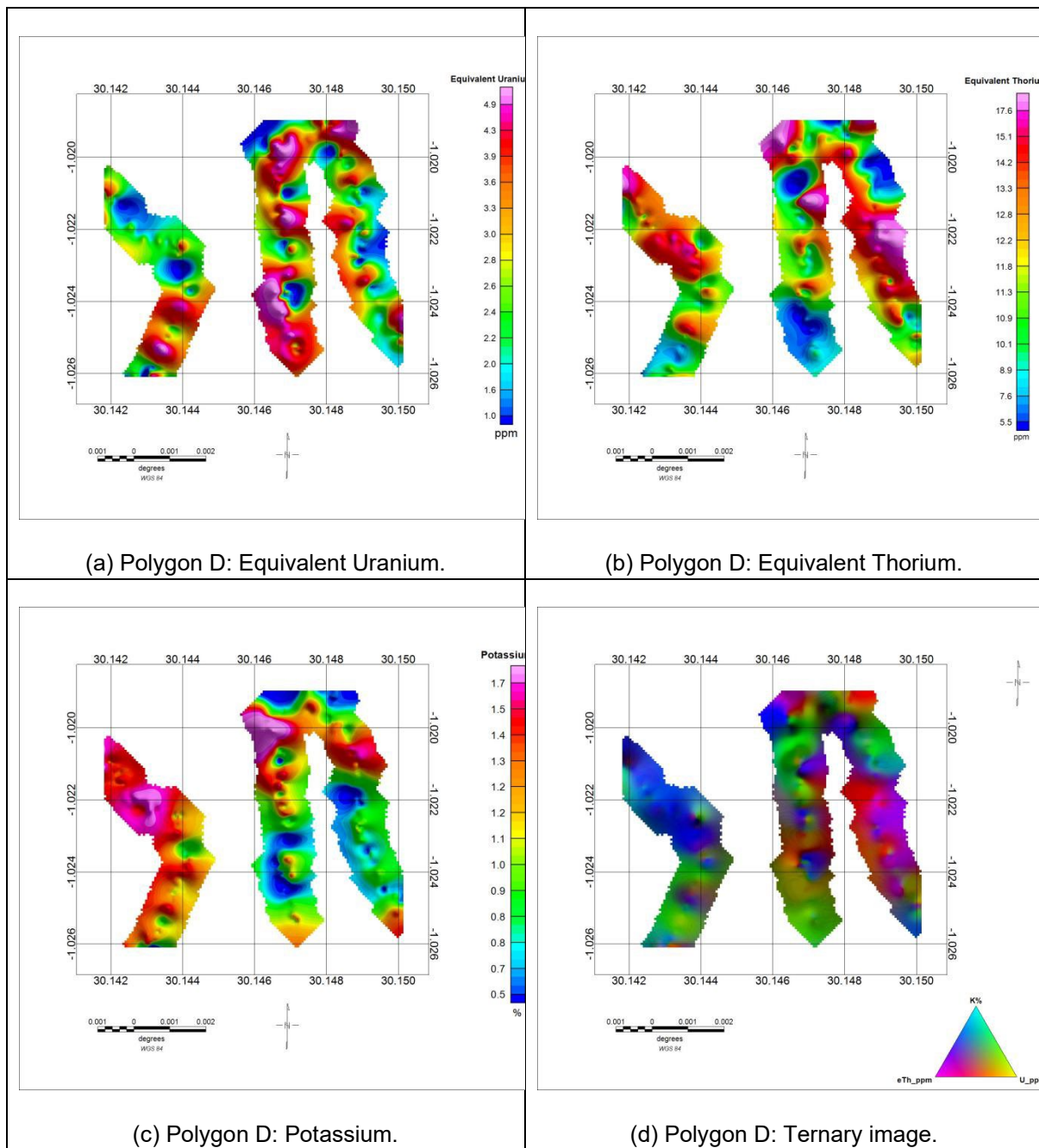


Figure 29. Radiometric maps for Polygon D.

2.4.7. Results of the geophysical survey

The magnetic data interpreted here were previously acquired from the Muko area close to Polygon B, located further south-western of Kabale. This is because the magnetic data from rover walkmag used in Polygon D failed to dump. The magnetic dataset analysed here indicate a high magnetic anomaly north of the survey area and magnetic lows just slightly below the high zone, this magnetic anomaly starts to rise up towards the middle of the survey area (Figs. 21, 22) and it continues further southwards.

The gravity data in Figure 24 shows regions of low to high density variations to the west of the polygon. The high (warm colours) Bouguer anomalies coincide with topographic highs of the survey area although some are possibly associated with pegmatites. The distinct gravity anomaly possibly indicates weathered quartzite.

The ternary map (Fig. 29d) shows regions of elevated potassium to the west of the polygon possibly associated with pegmatite body. Areas deficient in potassium are mostly dominated by quartzites. Also, there are indication of elevated uranium to the west. The elevated uranium probably coincides with schists and slates near the diopside outcrops. However, in some places, Thorium was twice the values of uranium (25–30 ppm).

2.5. Geochemical sampling practice

The area in the vicinity of Kabale is used for demonstration of several important geochemical methods used during geological mapping. For description of these methods in detail and the sampling patterns, we refer to the geochemical exploration handbook provided for PanAfGeo by the Czech Geological Survey (a soft copy version, Seifert et al. 2004).

2.5.1. Stream sediment sampling

Metals and other elements are prone to adsorption to certain clay minerals. This property is used for the stream sediment sampling, that consists of the selection of the very fine-grained, clayey or muddy portions of a complex profile of alluvial deposits. We sample up to 200 grams of sieved material combined from several different parts of the selected sedimentary profile for analyses (Figs. 30, 31). The methods reflect distribution of most elements of interest with very good coverage.



Figure 30. Explanation to methodics of soil sampling. Mbarara Road



Figure 31. Panning for heavy minerals in the bedrock stream East of Kabale town.

2.5.2. Soil sampling

For this type of shallow soil horizon sampling, the soil sounding bar for heavy soils and the plastic sledge hammer were used. The sounding bar can sample soils down to 1 m depth, in the case of light and soft soils the bar can be extended to reach deeper horizons. The sample up to 0.5 kg of soil can be taken from the selected target horizons. According to soil type, specific types of auger heads can be selected to effectively extract the sample from the spot.

2.5.3. Biogeochemical sampling

Samples of several types can be taken from the areas where rocks in situ are covered by any type of sediment (e.g., the desert crust-like calcrete, large colluvial fans, shallow water continental sediments, marshes, or thick alluvial sediments in large river valleys). It benefits from the ability of plant roots to extract local elements from the rocks covered by any other material and use them in tissues of leaves, bark, or fruits, or concentrate them in these parts of the plant, or even select some metal elements preferentially.

Another method used in dry areas is to sample the termite nests, where the material from the deep parts of the quaternary sediment is available at the surface, the higher above the ground, the deeper is the source. Materials are sampled and analysed by common analytical laboratory methods.

2.5.4. Heavy mineral sampling (HM)

The practical training of panning for heavy mineral concentrates from local sources are demonstrated and practised. Depending on target heavy minerals, various shapes of concentrators and sieves can be used during the exploration stages, also different materials can be combined. For the training, few sieves, Estwing plastic pans of various diameters, and the iron pan of 'Chinese hat' shape was used for concentrating. Magnetic fraction was separated on spot, reducing ferromagnetic fraction in the concentrate, while non-magnetic and paramagnetic fraction was kept for the microscopical mineralogical inspection in the DGS. Fine gold and pyrope garnet together with Fe-rich coarse-grained heavy minerals and limited other accessories from the local river were examined. The method provides either information on typical heavy accessory minerals specific of dominant source rocks important for mapping, or exploration data on the resistant heavy minerals indicating different types of mineralization (e.g., gold, PGE, Sn-W, some sulphidic types, F-Ba, REE) or on most gemstone occurrences (e.g., topaz, corundum varieties, diamond, gem garnets, kyanite...).

Panning locality: a steep stream valley near the village of Nkumbura

(WGS84: 01.242778° S, 030.095227° E)

The riverbed is eroded in the steep and narrow part of the valley with exposures of metasediments. It shows an ideal bedrock type stream with numerous natural traps for heavy minerals (behind in situ rock benches, big loose blocks, cobble accumulations with gravel and/or clayey sediment). The local material was tested for HM occurrences and showed predominance of Fe-bearing heavies like hematite and limonite with some limited proportion of zircon and monazite. For training purposes only, it was "salted" with imported flat gold flakes below 2 mm in diameter and small grains of pyrope garnet ("Bohemian garnet").

3. MINE EXCURSIONS

3.1. Iron mine Karukura

(U06, WGS84: 01.138866° S, 029.911288° E)

Iron ore quarry Karukura, covers the area about 150 m long and 30–50 m wide of rather irregular shape in a steep slope (Fig. 32). Hematite-rich domain is a part of the Mesoproterozoic Akanyaru-Ankole Supergroup. Ore body forms a hematite-rich concordant, relatively steeply dipping layer within grey clayey shales to clays from which hematitic body is separated by sharp contact. The direction of the layer is N–W, thickness is about 10 m, perhaps there are larger lenticular bodies stretched along one horizon. It is the same material as at the locality 1. Hematite breaks up by gravity into large blocks that run or slide over the soft clay. Workers break them with sticks and also use fire setting for softening of hard block. Very pure hematite is extracted, there is only little admixture of impurities below 5%. The ore is completely non-magnetic. It is a silver-grey very hard massive or fine-grained hematite with a conchoidal or uneven fracture. In addition to the most common massive hematite, there is also a rarer occurrence of cavities with well-formed lenticular hematite crystals up to 1 cm. Other minerals consist of quartz as small cavity fillings, sometimes also as 0.2–4 mm large, often bipyramidal crystals. There is also fine-grained flaky mineral of whitish silvery colour, which was determined by XRD as laumontite with an admixture of kaolinite. Upper in the subsoil, there is a bed of sandstone covered by clay. In addition, following minerals were determined on the hematite sample: dominant hematite, minor muscovite, kaolinite and probably Fe-rich amphibole.



Figure 32. Hematite mine hosted by low-grade slates and claystones, Karukura.

3.2. The tin mine of Mwerasandu, SE of Ntungamo

(U24, WGS84: 00.997122° S, 030.387662° E)

The historical Mwerasandu mine is one of the most famous tin operations in the Kabale area. It was opened around 1926 and was active until the 60ties by several galleries in four

underground levels and numerous diggings following mineralized structures or enriched slope sediments from the top. Only artisanal small-scale mining (ASM) continued since the mine closed. Now, a new company bought the license and plans to re-open the mine and establish new-type modern mine operating in accord with the green policy. It focuses on gravitational processing of ore, systematic recycling of all grey water, re-processing of clays, sand and gravels for local purposes, and reclaim exhausted parts of the area for agriculture. Most of local miners and other staff people are employed here.

The visit of the PanAfGeo group is organized in cooperation with the recent owners of the license.

Cassiterite mineralization is associated with several parallel subvertical quartz-tourmaline and pegmatite veins hosted by phyllite. These veins are zoned, enriched by coarse-grained and in places highly kaolinized micaceous domains containing cassiterite nodules and aggregates up to several centimeters. Light mica is enriched in Beryllium and rarely Lithium in specific zones. Occasionally, also ferberite partially replaced by limonite can be encountered in quartz-rich domains. Feldspathic zones are deeply kaolinized as well.

Relatively soft kaolinized cassiterite-rich domains are selectively mined from the mineralized structures, crashed and hand-washed by local miners. New small plant has been recently installed to process old tailings. A more productive processing gravitational unit is planned for underground operations.



Figure 33. Subvertical tourmaline and quartz vein in the host refoliated schists, Gallery No.8., Mwerasandu.



Figure 34. The ASM operation for alluvial tin placer beneath the Mwerasandu hill.

3.3. Tungsten-bearing pegmatite near Kacherere

(U12, Polygon D, WGS84: 01.022715° S, 030.137258° E)

During mapping, an abandoned mine NW of the Kacherere village was prospected. The mine closed in 60ties of the last century, and is mostly known as a source of tungsten-bearing mineralization hosted by pegmatite. There are at least three registered openings of the pegmatite body in three depth levels. The upper level was mined through an elongated surface digging transecting the host calc-silicate along at least 120 m long, 3 to 5 m wide and some 8 m deep open cut. A mid-level entrance is an ASM adit of about 40 m in length, and the lowermost main old gallery is accessible from the gully in the NW edge of the village. It is at least 200 m long gallery with irregular and inclined section of some 50 m in length, continuing

by straight regular vaulted profile with several short side drives few meters long, indicating the minimal thickness of the pegmatite body of 5 to 8 m at least in this deeper level.

Local miners focus on irregular pockets of fine-grained softer yellowish micaceous clay-rich material with black grains of ore minerals disseminated in matrix. Large flat crystals of biotite up to 10 cm are rarely present in marginal parts of the dyke and may indicate multiple pulses of pegmatite formation.

In some distance from the main pegmatite body to the NE, along the northern limit of the resistant calc-silicate body, parallel or irregular quartz veins with dark-brown limonitized mineralization occur. These quartz veins of variable thickness up to 1 m are accompanied by a massive darker alteration of schists (hypothetically tourmalinization).



Figure 35. Pegmatite near Kacherere: the surface open cut (top); the central part of the main gallery with the side prospecting drive in a kaolinized wall (left), a tourmaline-rich domain in the wall of the lower main gallery (right).



Pegmatite body is steeply inclining to the S, with predominantly E–W trending main part of the dyke. Pegmatite dyke is mostly without any apparent simple zoning, its internal structure is irregular, with varying proportions of K-feldspar, white quartz, predominating coarse-grained muscovite or other light mica, black tourmaline, secondary clay minerals, and some ore minerals in patchy or linear fine-grained domains. Fragments of large monocrystals of K-feldspar, quartz, muscovite and tourmaline are also disseminated in partially recultivated mining dumps in the upper part of the mine together with smaller pegmatite debris, and along the village roads often paved with excess gravel from the mine.

4. MAPPING AREAS/POLYGONS

The mapping area is located in the NW and NE vicinity of the town of Kabale in the SW tip of Uganda, near the border with Rwanda and Congo. Five polygons were delineated according to Fig. 36.

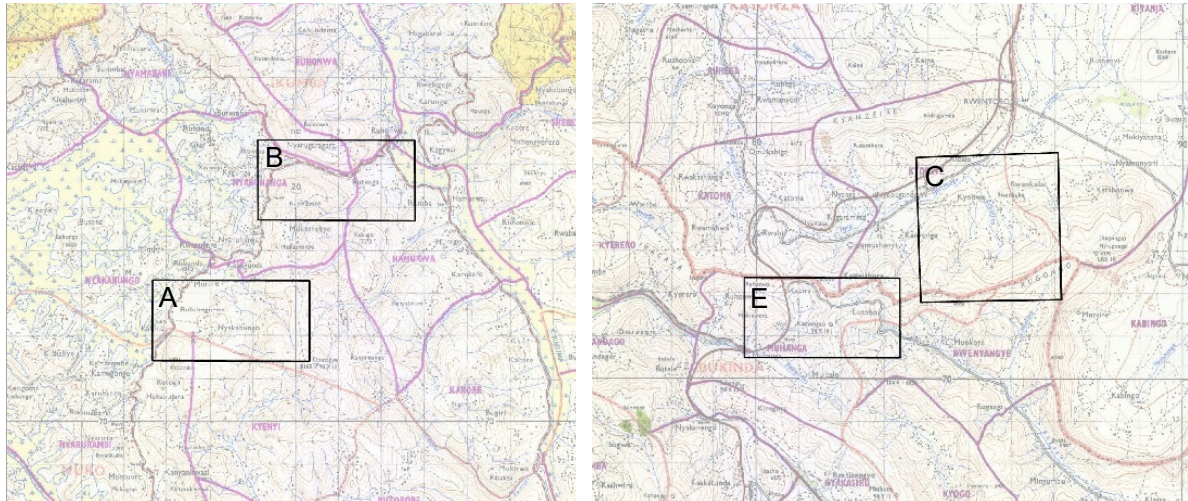
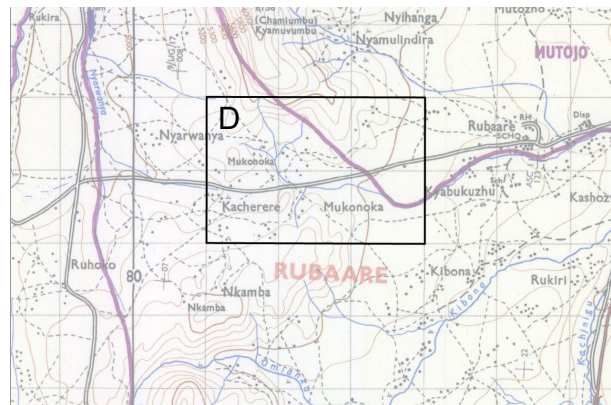


Figure 36. Mapping polygons delineated in the north-west (A, B), north-east (C, E) and northern (D) parts of the Kabale District. Shown on the Topographic map 1: 50 000.



5. REMOTE SENSING AND MOBILE METHODS

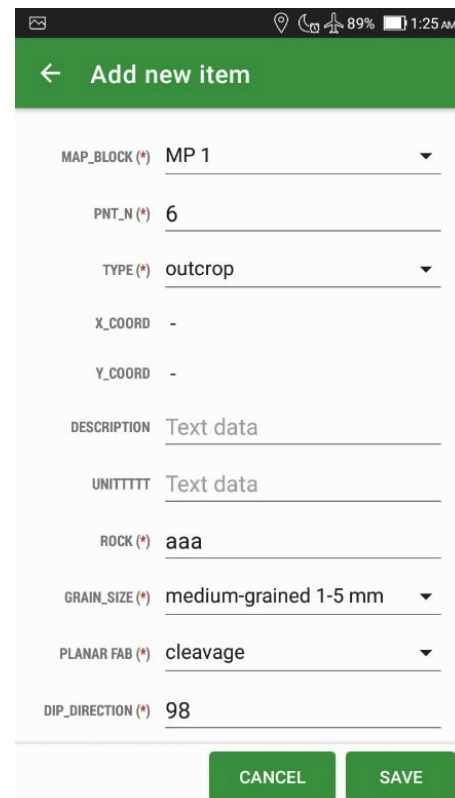
5.1 Field data collection using mobile app

To ensure geological mapping and data acquisition are recorded in a uniform way by all participants, the mobile application is used to collect field information. It was decided to use the free version of the Locus GIS Android application which is available in the Google Store. The mobile application provides offline display of the 1: 25 000 topographic map and orthophoto images of selected mapping areas (Fig. 37).

The important part is presented by the point vector layer that is structured to the form with attributes necessary to acquire in the field (Fig. 38). The preparation of the input data and the appropriate setup of the mobile application have been practiced and the data collection are sufficiently tested by all participants during the training.



Figure 37. Mobile app with background maps.



MAP_BLOCK (*)	MP 1
PNT_N (*)	6
TYPE (*)	outcrop
X_COORD	-
Y_COORD	-
DESCRIPTION	Text data
UNITTTTT	Text data
ROCK (*)	aaa
GRAIN_SIZE (*)	medium-grained 1-5 mm
PLANAR FAB (*)	cleavage
DIP_DIRECTION (*)	98

Figure 38. Point layer attribute structure.

5.2 Introduction to remote sensing methods

Remote sensing data have been a useful source of information to explore geology during the last few years. Participants were taught the basic principles of remote sensing methods, different types of remote sensing data, and free sources of satellite data available worldwide. Optical multispectral data of Sentinel-2 and ASTER images were downloaded and pre-processed in advance for further analysis. During the training, the whole chain of pre-processing steps is shown, including band stacking, clipping and masking. Basic band combinations, indices, and PCA transformation of Sentinel-2 and ASTER multispectral images are practiced, tested, and used for better recognition of lithological trends in the landscape

(Fig. 39). Remote sensing data were processed and observed in QGIS environment. This software was used for downloading and visualizing of the field data database and together with remote sensing data used to interpret geological map.

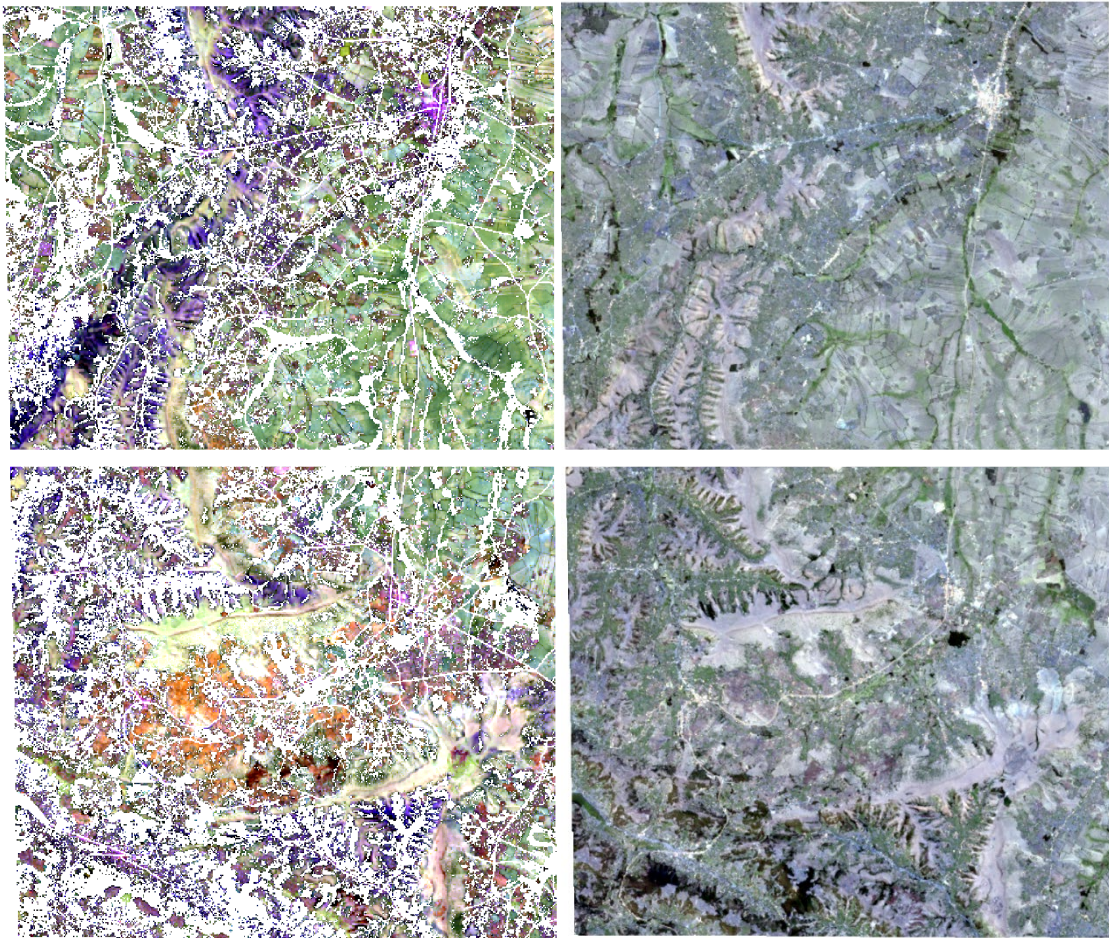


Figure 39. Processed (left) and unprocessed (right) Sentinel-2 data of the eastern mapping area near Kabale.

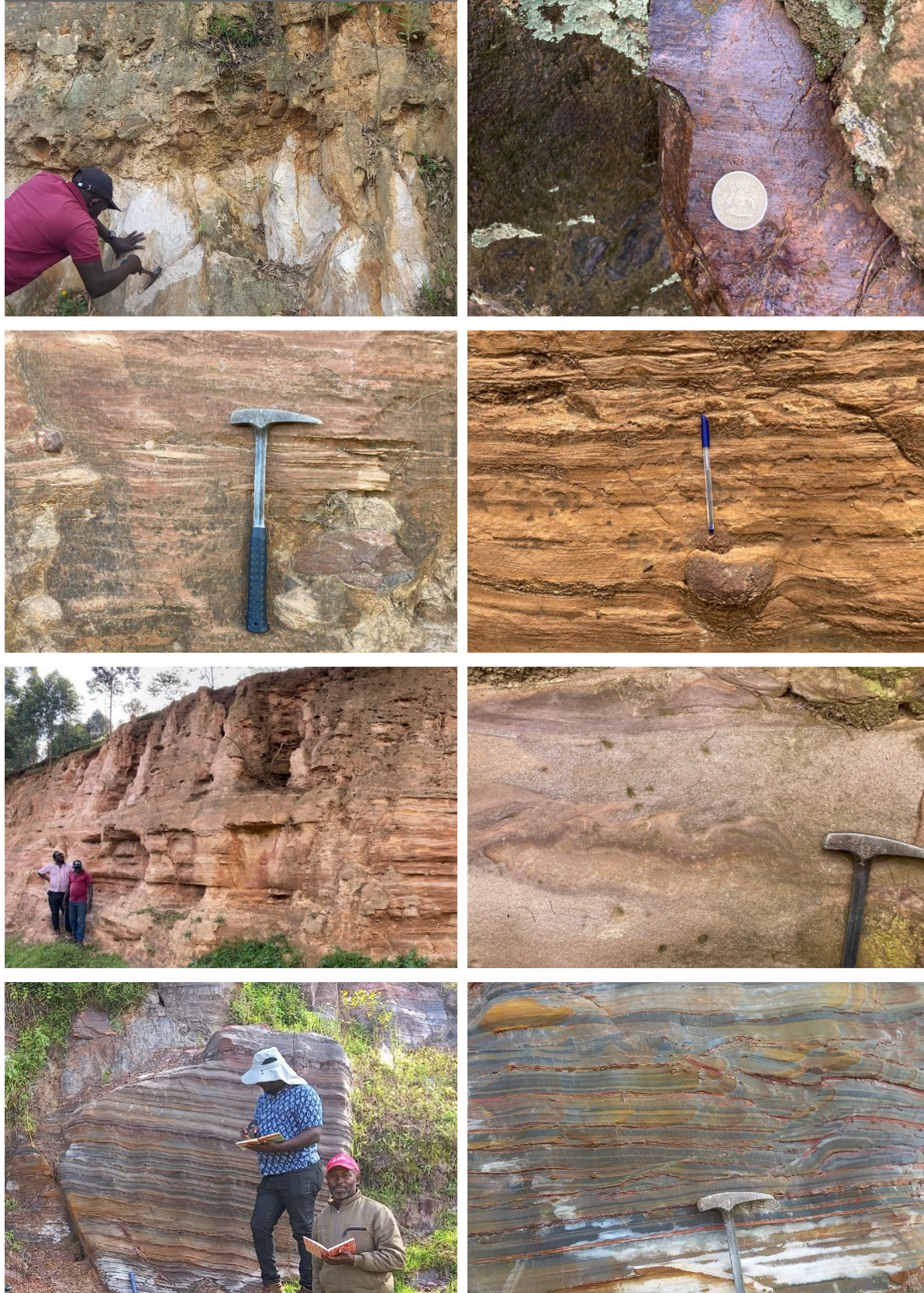
6. PLATES 1–7: LITHOLOGY OF THE TRAINING AREA

Plate 1 – Mesoproterozoic sediments of the Kabale area



a – slates with ripple marks; b – volcaniclastic breccia; c – weakly refoliated schists; d – brecciated clasts in sandstone; e – garnet micaschists, f – staurolite micaschists, NE of Kacherere; g – metaconglomerate; h – metamorphosed breccia, all Mbarara Road.

Plate 2 – Neoproterozoic rocks of the Kabale area



a – basal conglomerate overlaying MPTz quartzite; b – glacial striations on MPTz bedrock walls; c, d – dropstones in fine-grained laminated claystone; e – subhorizontally deposited laminated glaciolacustrine sediments; f – soft sediment structures in claystone; g, h – thin laminated claystones with syngedimentary slip and cross-bedding structures of uncertain age, all from Mbarara Road.

Plate 3 – Granitoids of the Neoproterozoic age



a – an intrusive contacts between leucogranite and Bt granite; b – Bt granite with lithoclasts of metasediments, c – fresh biotite granite, d – porphyritic granite, e – fine-grained leucocratic granite, f – deformed fine-grained granite with Qtz veinlet; g – tourmaline-bearing pegmatitic facies, all from outcrops along Mbarara Road; e – tourmaline-rich granite underlying volcanics at Kikombi.

Plate 4 – Dyke rocks



a – pegmatite vein in granite; b – quartz vein in phyllite; c – bothryodal limonite coating in open vugs in quartz veins ; d – turmalinite and quartz hydrothermal dyke in the Mwerasandu mine; e – minor vugs in hematite-rich Qtz vein; f – hematite-rich portion in quartz vein, the Kacherere sandstone quarry.

Plate 5 – EARS volcanic rocks of Neogene to Quaternary age



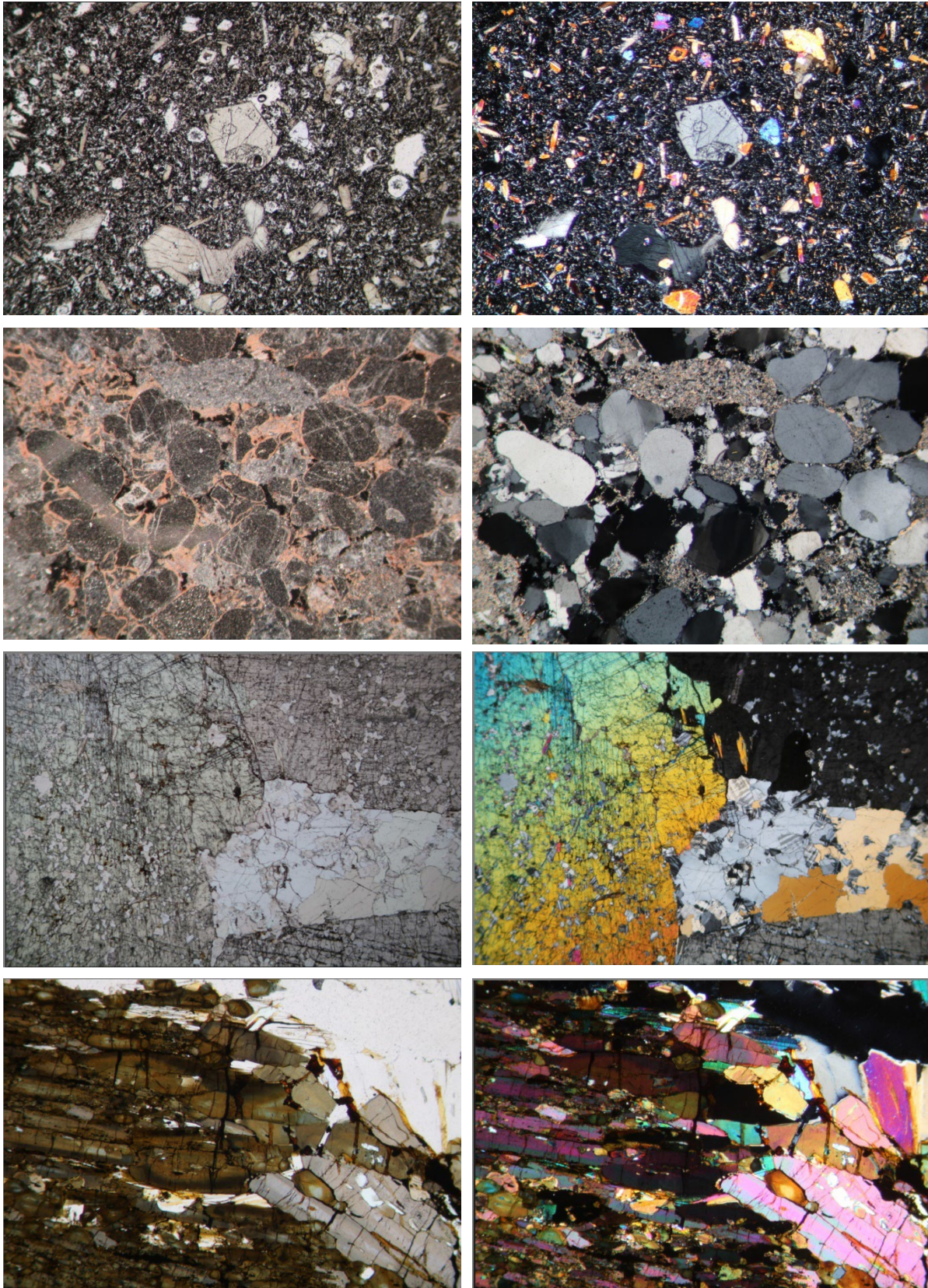
a – volcanoclastics quarried near Kyanika, Rwandan border; b – Kikombi volcano view with a quarry in pyroclastic fall deposits; c – detail of layered scoria fall deposits; d – scoria fall overlying vesiculated lava, e – massive lava with chilled scoria bombs fallen into the lava flow; f – scoria, g – recrystallized xenolith of granite, h – a bomb with breadcrust cooling surface; b–h Kikombi quarry.

Plate 6 – Quaternary sedimentary cover



a – a thermal spring and associated gas emanations, Nyamabaare Valley; b – a fluvial plain of the Nyamabaare river NW of Kabale; c – recent beach accumulation of hematite, Lake Victoria in Entebbe; d – laterite profile above metasediments, Mbarara Road; e – laterite soils and associated brick production; f – coluvia exposed in the Mbarara Road cut; g – a fossil river bed with fluvial conglomerate in palaeoterrace probably of Tertiary age (1920 m a.s.l., 400 m above recent valley, Polygon C - East); h – laterite crust, Polygon C East.

Plate 7 – Thin sections from Kabale area rocks



From the top: a, b – basanite from Kikombi Hill; c, d – sandstone, Kabale; e, f – diopside-rich Ca-Si rock, Kacherere; g, h – turmalinite, Kakanena. Left – PPL, right – XPL. Photomicrographs by Vladimír Žáček, CGS.

7. SELECTED BIBLIOGRAPHY

- Barnes, J.W. (1956). Precambrian structure and the origin of the granitoid rocks in SW-Uganda. PhD Thesis, University London, London.
- Bell, K. & Powell, J.L. (1969). Strontium isotope studies of the alkali rocks: the potassium rich lavas of the Birunga and Toro-Ankole regions, east and central equatorial Africa. *J. Petrol.*, 10, 536–572.
- Brinckmann, J., Lehmann, B., Hein, U., Höhndorf, A., Mussallam, K., Weiser, T. & Timm, F. (2001). La géologie et la minéralisation primaire de l'or de la chaîne Kibarienne, nord-ouest du Burundi, Afrique orientale. *Geologische Jahrbuch Reihe, D 101*, 3–195.
- Buchwaldt, R., Toulkeridis, T., Todt, W. & Ucakuwun, E.K. (2008): Crustal age domains in the Kibaran belt of SW-Uganda: Combined zircon geochronology and Sm–Nd isotopic investigation. *J.Afr. Earth. Sci.*, 51, (1), 4–20.
- Cahen, L., Snelling, N.J., Delhal, J. & Vail, J.R. (1984). The geochronology and evolution of Africa, Clarendon Press Oxford, 512 pp.
- Combe, A. & Simmons, W.C. (1933). The volcanic area of Bufumbira. Part I: The geology of the volcanic area of Bufumbira, south-west Uganda. *Memoir Geol. Surv. Uganda*, 3, 1–150.
- Dewaele, S., Henjes-Kunst, F., Melcher, F., Sitnikova, M., Burgess, R., Gerdes, A., & Lehmann, B. (2011). Late Neoproterozoic overprinting of the cassiterite and columbite-tantalite bearing pegmatites of the Gatumba area, Rwanda (Central Africa). *Journal of African Earth Sciences*, 61(1), 10–26.
- Fernandez-Alonso, M. & Theunissen, K. (1998). Airborne geophysics and geochemistry provide new insights in the intra-continental evolution of the Mesoproterozoic Kibaran Belt (Central Africa). *Geol. Mag.*, 135, 203–216.
- Hulsbosch, N., Boiron, M. C., Dewaele, S., & Muchez, P. (2016). Fluid fractionation of tungsten during granite–pegmatite differentiation and the metal source of peribatholithic W quartz veins: Evidence from the Karagwe-Ankole Belt (Rwanda). *Geochimica et Cosmochimica Acta*, 175, 299–318.
- King, B.C. (1942). An outline of the geology of southern Buwekula with adjoining portions of the Singo and Mawogola. Unpubl. Rept. Geol. Surv. Uganda, Entebbe, No. BCK/16.
- Klerkx, J., Liégeois, J.-P., Lavreau, J. & Claessens, W. (1987). Crustal evolution of the Northern Kibaran Belt, Eastern and Central Africa. In: Kröner, A. (ed.): *Proterozoic Lithospheric Evolution, Geodynamics*.
- Koegelenberg, C. & Kisters, A.F.M. (2014). Tectonic wedging, back-thrusting and basin development in the frontal parts of the Mesoproterozoic Karagwe-Ankole belt in NW Tanzania. *Journal of African Earth Sciences*, 97, 87–98.
- Kokonyangi, J.W., Kampunzu, A.B., Armstrong, R., Yoshida, M., Okudaira, T., Arima, M. & Ngulube, D. A. (2006). The mesoproterozoic kibaride belt (Katanga, SE DR Congo). *Journal of African Earth Sciences*, 46 (1–2), 1–35.
- Lenoir, J.L., Liégeois, J.P., Theunissen, K. & Klerkx, J. (1994). The Palaeoproterozoic Ubendian shear belt in Tanzania: geochronology and structure. *Journal of African Earth Sciences*, 19(3), 169–184.
- Mäkitie, H., Data, G., Isabirye, E., Mänttari, I., Huhma, H., Klausen, M. B. & Virransalo, P. (2014). Petrology, geochronology and emplacement model of the giant 1.37 Ga arcuate Lake Victoria Dyke Swarm on the margin of a large igneous province in eastern Africa. *Journal of African Earth Sciences*, 97, 273–296.
- Mänttari, I. (2010a). Radiometric ages for rock samples from Uganda. Sustainable management of mineral resources project. Report 3, 2010. GTK Consortium. 37 p., 1 App.
- Mänttari, I. (2010b). Radiometric ages for rock samples from Uganda. Sustainable management of mineral resources project. GTK Consortium, Report 4, 46 p., 1 App.

- Melcher, F., Graupner, T., Gäbler, H.E., Sitnikova, M., Henjes-Kunst, F., Oberthür, T. & Dewaele, S. (2015). Tantalum–(niobium–tin) mineralisation in African pegmatites and rare metal granites: Constraints from Ta–Nb oxide mineralogy, geochemistry and U–Pb geochronology. *Ore Geology Reviews*, 64, 667–719.
- Tack, L., Duchesne, J.-C., Liégeois, J.-P. & Deblond, A. (1994). Kibaran A-type granitoids and mafic rocks generated by two mantle sources in a late orogenic setting (Burundi). *Precambrian Res.*, 68, 323–356.
- Tack, L., Fernandez-Alonso, M., Dewaele, B., Tahon, A., Dewaele, S., Baudet, D. & Cutten, H. (2006). The Northeastern Kibaran belt (NKB): a long-lived Proterozoic intraplate history. *Extended Abstract, 21st Coll. Afr. Geol. (CAG21)*, Maputo, 3–5 July 2006, 149–151.
- Tack, L., Wingate, M.T.D., Dewaele, B., Meert, J., Griffin, B., Belousova, E.A., Tahon, A., Fernandez-Alonso, M., Baudet, D., Cutten, H.N.C. & Dewaele, S. (2008). The Proterozoic Kibaran Belt in central Africa: Intracratonic 1375 Ma emplacement of a LIP. *Abstract, 22nd Coll. Afr. Geol. (CAG22)*, 4–6 November 2008, Hammamet, Tunisia, 89.
- Tack, L., Wingate, M.T.D., De Waele, B., Meert, J., Griffin, B., Belousova, E.A., Tahon, A., Fernandez-Alonso, M., Baudet, D., Cutten, H.N.C. & Dewaele, S. (2009). The Mesoproterozoic “Kibaran Event” in Central Africa: a 1375 Ma intracratonic emplacement of a Large Igneous Province (LIP). *Geol. Soc. London, Fermor Meeting “Rodinia: Supercontinents, superplumes and Scotland”*, Edinburgh, 9–13 Sept. 2009.
- Tack, L., Wingate, M.T.D., De Waele, B., Meert, J., Belousova, E., Griffin, B., Tahon, A. & Fernandez-Alonso, M. (2010). The 1375 Ma “Kibaran event” in Central Africa: Prominent emplacement of bimodal magmatism under extensional regime. *Precambrian Research* 180, 63–84.
- Van Daele, J., Hulsbosch, N., Dewaele S., Muchez P. (2020). Metamorphic and metasomatic evolution of the Western Domain of the Karagwe-Ankole Belt (Central Africa).
- Westerhof, A.B. (2012). Summary Report on the Geology and Geodynamic Development of Uganda.
- Westerhof, A.B., Pekkala, Y. & Lehto, T. (Editors) Elepu, D., Härmä, P., Koistinen, T., Kuivasaari, T., Kärkkäinen, N., Lehtonen, M.I., Manninen, T., Mäkitie, H., Pokki, J., Saalman, K., Staudt, M. & Virransalo, P. (2011): EXPLANATION OF THE GEOLOGY OF SHEET SA-36-5 (Kabale) 1: 250 000.
- Westerhof, A.B., Pekkala, Y. & Lehto, T. (Editors) Baglow, N., Boger, S., Elepu, D., Härmä, P., Jenett, T., Koistinen, T., Kuivasaari, T., Kyagulanyi, D., Kärkkäinen, N., Lehtonen, M.I., Manninen, T., Mäkitie, H., Pokki, J., Schumann, A., Staudt, M. & Virransalo, P. (2011): EXPLANATION OF THE GEOLOGY OF SHEET SA-36-1 (Mbarara) 1: 250 000.



Figure 40. The WPA-U5 group on the top of the Mwerasandu hill and the tin mine, 2024.

8. WPA-U5 PARTICIPANTS

No	Last name	First name	Country
Mr	MACHUKA	Onkgopotse Mpinda	Botswana
Mr	AHMED HAMDY	Youssef Ali	Egypt
Dr	HOSSAMELDIN KHAIRY	Hussein Sharaka	Egypt
Mr	GHEBREWELDI	Abel Yacob	Eritrea
Mr	HAGOS	Kokob Mebrahtu	Eritrea
Mr	JAL	Jamuth Pajock	Ethiopia
Mr	JIRU	Melese Tute	Ethiopia
Mr	TEKIA	Teklay Gidey	Ethiopia
Mr	ASARE	Michael Seli	Ghana
Ms	BEKOE	Doreen	Ghana
Mr	OBUYA	Walter Otieno	Kenya
Ms	FALLAH	Cecelia Finda	Liberia
Mr	CUMBANE	Felix Arnaldo	Mozambique
Ms	OGUNTIMEHIN	Theresa Muyiwa	Nigeria
Mr	UWIMANA	Jean Nepomuscene	Rwanda
Mr	Mahgoub Siddig	Mohamed Adam	Sudan
Mr	Moahmmeddiaeldeen Mubarakhajmoussa	Mohammed Ahmed	Sudan
Ms	HASSAN	Hidaya Omari	Tanzania
Mr	TAMAMBELE	Ambaliche Leo	Tanzania
Mr	MULINDWA	Henry	Uganda
Ms	NANKINGA	Stella	Uganda
Mr	OLWA	James	Uganda
Mr	UZATUNGA	Paul Brian	Uganda
Mrs	CHINAKA	Kweshwa	Zambia
Mr	MWILA	David Abel	Zambia
Experts	Trainers and officials CGS and DGS Uganda		
26	Veronika Štědrá	Coordination/Gch	Czechia
27	Vladimír Žáček	Map, legend, geology	Czechia
28	Jan Jelének	RS/GIS	Czechia
29	Zuzana Tasáryová	RS/Map/Sedimentology	Czechia
30	Pavel Pitra (Univ. Rennes)	Met. petrology/Structural	Czechia, France
31	Joseph Aiykobua	RS/Mapping/Coordination	Uganda
32	Sudan Unity Birungi	Mapping	Uganda
33	Nelson Birungi	Geophysics - gravi, geoel.	Uganda
34	Joseph Nyagi	Geophysics - geomagnetics	Uganda
35	Deus Katomi	Geochemistry	Uganda
36	Edward Marimira	Petrology	Uganda
37	Grace Lajwe	Laboratory methods	Uganda
38	Gabriel Data	OAGS representative, DGS	Uganda